Journal of Hydrology 458–459 (2012) 68–86

Contents lists available at SciVerse ScienceDirect

Journal of Hydrology

journal homepage: www.elsevier.com/locate/jhydrol

Probabilistic flood inundation mapping of ungauged rivers: Linking GIS techniques and frequency analysis

Ali Sarhadi [a,*], Saeed Soltani [a], Reza Modarres [b]

[a] Department of Natural Resources, Isfahan University of Technology, PO Code 8415683111, Isfahan, Iran
[b] Institute national de la recherche scientifique, 490 rue de la couronne, Québec (Québec), Canada

ARTICLE INFO

Article history:
Received 3 October 2011
Received in revised form 10 June 2012
Accepted 20 June 2012
Available online 28 June 2012
This manuscript was handled by Andras Bardossy, Editor-in-Chief, with the assistance of Axel Bronstert, Associate Editor

Keywords:
Flood hazard mapping
Ungauged reaches
High resolution Cartosat-1 based DTM
HEC RAS
Flood frequency analysis
Arid regions

SUMMARY

This study presents an exhaustive methodology of floodplain mapping at ungauged rivers. To present our methodology, we selected the Halilrud basin and Jiroft city in southeastern Iran as an example of hazardous regions. To estimate flood quantiles in different return periods at ungauged reaches, we used regional flood frequency analysis. By using the well-known L-moments approach and related criteria, a homogeneous region was formed and the 3-parameter Log normal distribution was identified as the robust regional frequency distribution. The hydro-geomorphic characteristics and the land use properties of the catchments were then extracted using RS&GIS techniques to establish multivariate regional regression models between hydro-geomorphic characteristics and flood quantiles. After delineation of the catchments for the ungauged reaches, flood quantiles as an important factor in flood inundation at outlets of these reaches with different probabilities were estimated using the regional regression models. To delineate flood hazard maps and to enhance the accuracy of the hydraulic modeling, we applied satellite stereoscope images of Cartosat-1 along with the Rational Polynomial Coefficients to extract a high resolution DTM and detailed parameterization of the channel required by 1D hydraulic model HEC-RAS. The GIS-based HEC-Geo RAS pre- and post-processor were also used for careful optimization of the geometry features for real visualization of the flood prone areas. Information of some historical flood events was also used to evaluate the hydraulic model performance in predicting flood inundations. Finally, vulnerable areas were crossed with extracted land use mapping from IRS-P6 satellite images to differentiate the critical infrastructures and the valuable land use classes affected by floods in different return periods.

1. Introduction

Floods are among the most devastating natural disasters in the world, claiming more than 20,000 lives per year and adversely affecting about 75 million people world-wide, mostly through homelessness (Smith, 2001). As the severity and frequency of flood events have considerably increased, there is a growing global concern about the need to decrease flood related fatalities and associated economic losses. Identifying prone areas can therefore be one of the key solutions in flood mitigation. Predicting susceptible floodplains and high potential flash flood prone areas can help authorities in planning management strategies for flood mitigation such as designing water control structures (reservoir levee projects), decision making for flood insurance and facilitating emergency preparedness to cope with flooding (Sanders, 2007; Srinivas et al., 2008).

To identify flood prone areas, a model is required to predict spatially distributed estimates of the hydraulic variables such as flood inundation extent and depth. 1D and 2D dimensional hydraulic models are now widely used for this purpose. These models are able to compute water surface profiles rapidly in several different characterizations of the system. Recently developed tools for hydraulic modeling are Geographical Information System (GIS) (Casas et al., 2006; Merwade et al., 2008) and Remote Sensing (RS) techniques (Chormanski et al., 2011; Straatsma and Baptist, 2008) that allow one or two-dimensional representation of the computed hydraulic parameters. In hydraulic modeling, two critical factors: (i) streamflow data (flood quantiles), and (ii) topography of river channel (Horritt and Bates, 2001) influence flow hydraulics and the resultant areal extent of the simulated flood inundation.

Almost all studies in identifying floodplain inundation areas have been carried out at gauged rivers or have been done based on available flow information of upstream station(s) (Aggett and Wilson, 2009; Bates et al., 2006), even though many flood prone regions include large population centers or precious land uses suffer from a lack of site-specific records upstream. The lack of data for ungauged rivers often deprives researchers to have an accurate prediction of flood magnitude as a key factor for a reliable flood inundation mapping.

* Corresponding author. Tel.: +98 311 3912841x1029; fax: +98 311 3912840.
E-mail address: alisarhadi2005@gmail.com (A. Sarhadi).

0022-1694/$ - see front matter © 2012 Elsevier B.V. All rights reserved.
http://dx.doi.org/10.1016/j.jhydrol.2012.06.039

Nomenclature

DEM	Digital Elevation Model
DGPS	Differential Global Positioning System
DTMs	Digital Terrain Models
GCPs	Ground Control Points
GIS	Geographical Information System
LCk	L-Coefficient of Kurtosis
LCs	L-Coefficient of Skewness
LCv	L-Coefficient of variation
LiDAR	Light Detection and Ranging
MDP	Maximum Daily Precipitation
LMRDs	L-Moment Ratio Diagrams
MRRA	Multivariate Regional Regression Analysis
MRRMs	Multivariate Regional Regression Models
RFFA	Regional Flood Frequency Analysis
RPCs	Rational Polynomial Coefficients
RS	Remote Sensing
SAR	Synthetic Aperture Radar
VIF	Variance Inflation Factor

Flood magnitude prediction at ungauged reaches is an important task in designing river engineering and hydraulic structures and remains a fundamental challenge for hydrologists (Li et al., 2010). At ungauged basins, hydrological regionalization is usually applied as a reliable method for the estimation of the hydro-climatic variables at different return periods in the site of interest (Hosking and Wallis, 1997). Regionalization transfers hydrological information from one or more gauged catchments to geographically contiguous (or non-continuous) regions and hydrological neighborhood ungauged catchments of interest (Ouarda et al., 2001) by extrapolation using remote sensing data, hydrologic model simulation and integrated meteorological and hydrological modeling approaches (Goswami et al., 2006).

Regional Flood Frequency Analysis (RFFA) comprises two main steps: delineation of the groups or regions of the hydrologically homogenous catchments, and estimation of the regional flood quantiles at different return periods for the region of interest (Ouarda et al., 2006; Sarhadi and Modarres, 2011). The homogeneity of a group of sites is a fundamental requirement for performance of an effective regional estimation of the exceedance of the flood events (Castellarin et al., 2008). Hydrologists have proposed a number of tests and analyses to check the homogeneity of hydrological variables. One of the first statistical tests based on the variability of sample coefficients of variation and/or skewness among sites, was proposed by Dalrymple (1960). Then Lu and Stedinger (1992) suggested a homogeneity test according to the variability of normalized at-site Generalized Extreme Value (GEV) distribution flood quantiles. L-moments method introduced by Hosking and Wallis (1993) is now widely used by hydrologists to test the regional homogeneity of hydro-climatic variables. Hosking and Wallis (1993, 1997) proposed heterogeneity statistics for the estimation of the degree of heterogeneity in a group according to the intersite variability of L-moment ratios. In comparison to conventional moments, L-moments are superior to the product moments in that the former are more robust in the presence of outliers and less subject to bias estimation, and of course do not suffer from sample size related bounds as well.

To estimate the probability of the exceedance of the flood quantiles at the particular ungauged sites within each delineated homogenous region, several regional approaches have been established. Some of them consist of pooling hydrologically similar catchments into a homogeneous group and subsequently using averages within each pooling group to estimate flood probabilities in target catchments, such as the Index Flood (Dalrymple, 1960; Singh, 1992), and the Region of Influence (ROI) (Burn, 1990; Pfaundler, 2001) approaches. The other alternative approaches are based on application of geostatistical methods, which use spatial proximity as a measure of hydrological similarity (Merz and Blöschl, 2005). An extensive review and comparative evaluation of different regionalization methods is found in the study of GREHYS (1996).

Perhaps one of the earliest and the most widely used methods applied to estimate hydrological variables at ungauged sites is Multivariate Regional Regression Analysis (MRRA), which uses flood quantiles and catchment attributes (Chiang et al., 2002; Pandey and Nguyen, 1999; Vogel et al., 1999). In regional flood quantiles estimation, a power-form equation is generally used to relate flood quantiles of interest to catchment physiographic, geomorphologic and climatic characteristics. Because of their easy application, regional regression models have been recently applied not only for flood flow prediction at ungauged sites (Rao and Hamed, 1997; Vogel et al., 1993, 1999), but also for low flow prediction (Chen et al., 2006; Kroll and Vogel, 2002; Modarres, 2008) and hydrological drought analysis (Modarres and Sarhadi, 2010).

In this study, we link an L-moments approach and parametric regional regression models for flood quantile estimation via a catchment's characteristics. In this way, Multivariate Regional Regression Models (MRRMs) allows an estimation of the flood quantiles in different return periods at ungauged reaches of interest as probabilistic scenarios for simulating floodplain inundations.

Besides flood quantile estimation, the second issue in hydraulic modeling and predicting flood inundation mapping is the quality and accuracy of the topographic data source (Sanders, 2007). In flood hydraulic modeling, the resolution of the topographic data is a key element (Sanders, 2007), so small errors in topography affect the accuracy of the hydraulic model prediction (Aronica et al., 1998; Finlayson and Montgomery, 2004; Wilson, 2004). Traditionally, topographic surveys and manual interpretation of the terrain maps, which are limited by serious time and expense constraints (Marche et al., 1990; Nardi et al., 2006), were used as the only available method for terrain modeling. However, the availability of the digital terrain information and spatial modeling tools in GIS has made it possible for researchers to utilize Digital Terrain Models (DTMs) to investigate the effects of a channel's spatial variability on prediction of the flood hazard mapping. More recently, the advancement of RS technology has provided new capabilities that improve the quality of floodplain inundation mapping. The most promising data sources are Light Detection and Ranging (LiDAR) (Aggett and Wilson, 2009; Webster et al., 2004) and Synthetic Aperture Radar (SAR) data (Martinez and Toan, 2007; Schumann, 2007), which provide effective topographic datasets for the specific requirements of hydraulic modeling. Currently, the use of DTMs for hydraulic modeling is conditioned by their availability or by the economic factors (Cobby and Mason, 1999; Gomes Pereira and Wicherson, 1999). As high-resolution elevation data are costly and currently available for only a limited number of rivers, in this study we introduce an alternative remote sensing-based technique for extracting highly detailed topographic datasets that increase the accuracy of hydraulic modeling.

The aim of this study is to present an efficient methodology for the delineation of the flood hazard mapping at ungauged rivers.

Therefore, for this purpose, we use RFFA to predict flood quantiles in different probabilistic scenarios at ungauged rivers. A new remote sensing-based method is used for the extraction of the high resolution DTM using stereoscopic Cartosat-1 images in order to improve our understanding of the river geometry. Other GIS programs and techniques are also employed for hydraulic modeling to address areas which may be affected by flood events in different return periods.

This paper is organized as follows: Section 2 introduces the study area and describes the data set; Section 3 provides a brief overview of the methods of a RFFA and depicts flood inundation mapping; Section 4 presents the results of the applications of various techniques for addressing flood prone areas in different scenarios. Finally, a brief summary and conclusion end the paper.

2. Study area and data used

The Halilrud basin was selected as the focus for the present study. Located in an arid and semi-arid region, with an area of 1.6 Mha and 265 mm mean annual precipitation, the Halilrud basin is one of the vulnerable areas to flash flood damages in Kerman province in the southeastern territory of Iran. High mountain ranges and abrupt slope changes at the foot of mountains create special hydro-geomorphical characteristics for the Halilrud basin, making it a region vulnerable to the flooding. These conditions accompanied with shallow topsoil often lead to excess runoff due to rapid response of the catchments to intense rainfall.

This basin is among a mountainous area in the region. Generally, the elevation of the Halilrud basin declines from north to south. The upper and the middle parts of the basin include mountainous areas and downstream parts form a flat plain. The temporal distribution of the precipitation is irregular over the basin with a winter and spring rainy season, while heavy short storms are limited to summer. This condition, accompanied by impenetrable soils and highly sloped mountains, creates a special hydro-morphologic condition for this basin and increases the flooding hazard potential for the residential centers located in the flatted downstream territories.

One of the most important population centers in the Halilrud basin which suffers from flood damages is Jiroft city. This city and its territory are considered among the most strategic areas of Iran from an agricultural production point of view. Surrounded by high mountains, this city is located at the junction of two main ephemeral rivers, the Halirud and Shur (in the basin and originating from upstream mountains) Rivers, lying at the foot of the mountains, exactly at the end of mountainous parts (Fig. 1b and c).

One of Jiroft's most destructive flood events occurred in February 1993. This historical flood, which peaked up to 3800 m^3/s, killed 12 people and made 4200 others homeless. Furthermore, this catastrophe also destroyed the infrastructure of the city and affected residential, industrial and economic parts of Jiroft and its vicinity. The financial losses were estimated at about 20,000,000 $ (Sarhadi, 2008). Fig. 2 shows rare photos of this event.

In the present study, we consider a 10-km long reach of Halil River, an 8-km reach of the Shour River and a 3-km reach of the Malanti River passing through the center of the city, as a demonstration of the proposed methodology (Fig. 1c).

The data set includes an annual flood peak time series of 15 stations across the two main catchments of the Halilrud (the Hali and Shur). The location of these stations is illustrated in Fig. 1b. The circle size presents a scale for the area of each catchment. The annual peak flow data (as dependent variables), which are extracted from the streamflow data series of 15 stations, cover the time-span of 1970–2006 and come from the Iranian Ministry of Power. The time-span for the available flood data records is different, so the shortest length of data belongs to Kenaruieh station (13 years)

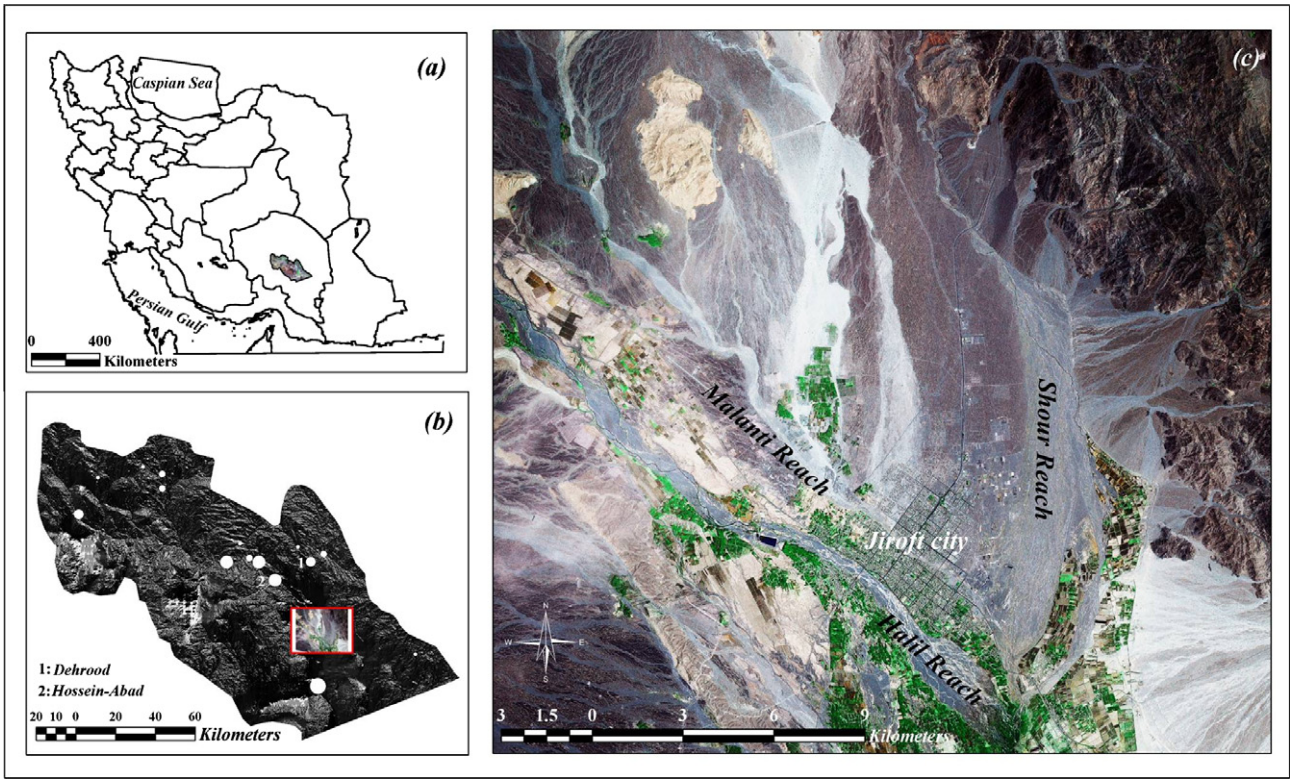

Fig. 1. Location of the study area: (a) position of the Halirud basin in Iran, (b) study stations (diameter of the circles is proportional to the catchment's area), and location of the nearest upstream stations to Jiroft city; 1: Dehrood station, 2: Hossein-Abad station, (c) study reaches and Jiroft city situation.

Fig. 2. Photos of the 1993 historical flood event in Jiroft city.

and the longest record belongs to Soltani station (36 years). The mean of the record length of all stations is 22 years. Table 1 shows the characteristics of the study stations. To establish regional regression models, we need to select independent variables. According to previous studies (Chokmani and Ouarda, 2004; Srinivas et al., 2008; Vogel et al., 1999), in addition to information of the drainage area, information on hydro-geomorphic, climatic and land use parameters are also required in explaining regional differences in annual streamflow. Therefore, to delineate the catchment's characteristics, some tools are used in RS&GIS environments.

In order to delineate flood hazard mapping of reaches surrounding Jiroft city, which is the aim of the present study, we need flood magnitudes in different return periods as a key factor. As it is apparent in Fig. 1b, the nearest stations to the city are Hossein-Abad in Halilrud catchment and Dehrood station in Shur catchment, both located in mountainous areas. Due to far distances of these stations from the study reaches and the division of the main rivers to the various branches just before Jiroft city as well as the existence of seasonal streamflows which feed these two main rivers (observable in Fig. 1c, which covers just a small part of the study rivers), flood data at these stations cannot describe flood characteristics at the study reaches passing through Jiroft city. In other words, the flood magnitude at these stations is significantly different from the flood flow magnitudes that occur in the mentioned ungauged rivers. Therefore, it is important to estimate flood magnitude in different return periods as a key issue in flood hazard mapping at the ungauged reaches under study. To do this, regional flood models are carried out.

2.1. Catchment boundary delineation

To extract catchment boundaries and hydro-geomorphic properties, an automated GIS-based procedure (Arc Hydro) is employed in ArcInfo (ESRI, 1990). This procedure uses topographic data (Digital Elevation Model (DEM) with 30 m resolution) for the identification of the stream networks using a constant area threshold for channel head locations (O'Callaghan and Mark, 1984). Surface flow paths are determined by the eight direction (D8) model (Nardi et al., 2006). After pit filling, the contributing area is divided for each cell. The stream network is identified by flagging cells draining more than one contributing area threshold (Nardi et al., 2006). To define a threshold, we need to map stream location. After full terrain processing and completing automated delineation of the network, the catchment's boundaries corresponding to the selected outlets (at the location of the stations) are then extracted. It must be noted that all of these processes are also possible in other extensions, such as HEC-GEO HMS.

Table 1
List of the study gauges and their characteristics in the Halilrud basin.

Station name	Code	Longitude	Latitude	Elevation (m)	Sample size (year)	Record period
Aroos	44-005	57–25	28–53	1250	14	1992–2006
Cheshme	44-150	56–52	29–18	2460	20	1986–2006
Dehrood	44-009	57–44	28–52	1000	34	1972–2006
Hanjan	44-053	56–58	29–16	2150	17	1989–2006
Hossienabad	44-007	57–33	28–47	920	35	1971–2006
Kahnak	44-011	57–46	28–18	520	21	1985–2006
Kaldan	44-027	57–40	28–56	1440	20	1986–2006
Kenarueih	44-115	57–18	28–52	1340	13	1993–2006
Meidan	44-111	56–58	29–12	519	21	1985–2006
Narab	44-21	57–28	28–52	1100	14	1992–2006
Polbaft	44-001	56–38	29–15	2200	26	1980–2006
Ramoon	44-107	57–22	28–57	1500	14	1992–2006
Soltani	44-003	56–32	29–05	2000	36	1970–2006
Tighsiah	44-035	58–16	28–27	1600	20	1986–2006
Zarrin	44-029	57–48	28–54	1400	22	1984–2006

2.2. Hydro-geomorphic and climatic characteristics

All of the important hydro-geomorphic variables selected for this work are selected based on previous studies (Chokmani and Ouarda, 2004; Srinivas et al., 2008; Vogel et al., 1999). These variables include Basin Area, Basin Slope (%), Mean and Maximum Elevation, Number and Length of the Specific River and River Slope. Meanwhile, other hydrologic variables derived from these basic variables, such as Drainage Density, Time of Concentration, Bifurcation Ratio, and Basin Shape Coefficient (Compactness coefficient), are also computed. All of the rivers' and watersheds' physical characteristics, which are stored in the previously mentioned hydrological parameters, are extracted by terrain processing on a DEM.

Since precipitation is an important climate element in watershed hydrology and hydrologic engineering planning, we use Maximum Daily Precipitation (MDP) an indicator of the climatic factors, as an independent variable in the regional regression models. All hydro-geomorphic and climatic characteristics used in this study are presented in Table 2.

2.3. Land use parameters

Due to the importance of the type of land uses and their roles in runoff generation, we used IRS-P6 satellite images for the extraction of the land use characteristics of the study catchments. To extract a land use map, elimination of or compensation for the atmospheric effects via some forms of calibration is particularly important (Jian and Mason, 2009). After pre-processing analyses of the multispectral data, supervised classification was carried out to extract land use classes. Briefly, in this method, total numbers of 76 training samples were selected. Fieldwork for the selection of training samples was carried out in 2007, only 1 year after satellite data acquisition. Eight signatures were generated from training samples, and the maximum likelihood classification was then performed. To manifest satellite images, different analyses such as fusion, creation of the best false color composite, principal component analysis and vegetation indices were applied to extract the specific land use classes (Jian and Mason, 2009). Finally eight land use classes which have key roles in flood generation, namely bare lands, range lands, forest area, agriculture, gardens, urban, lake (surface storage) and rock were extracted with an accuracy of 92%. The extracted land use map of the Halilrud basin is given in Fig. 3. The portion of the land use classes for each catchment was then assigned (Table 3).

3. Methodology

Since there is no comprehensive study to explain the complete process of flood inundation mapping at ungauged reaches, this study introduces a comprehensive methodology and explains the different stages needed in mapping flood prone areas at ungauged rivers. The proposed methodology consists of two major parts: the first part is RFFA, which uses a regional regression method as the regional estimation procedure to predict flood quantiles in rivers where no historical flood record is available. This part includes three steps (Hosking and Wallis, 1993, 1997): (1) delineating homogeneous regions, (2) selecting a robust regional frequency distribution function, (3) establishing regional flood models to obtain probabilistic flood quantiles at ungauged reaches. The second part is the simulation of the flood prone areas according to the estimated probabilistic flood quantiles in the previous part, which consists of two steps: (1) Terrain modeling of the river channel using a high resolution DTM, and (2) Hydraulic modeling. All of these stages are summarized in Fig. 4 and discussed in the following sections.

3.1. Regional flood frequency analysis

RFFA usually involves three steps of identifying regions of hydrologically homogenous regions, describing a robust regional probability distribution, and applying a regional estimation method within the identified homogenous regions (Hosking and Wallis, 1993, 1997). A multivariate regional regression model is often used for developing regional flood frequency models (Pandey and Nguyen, 1999). This method estimates flood statistics at ungauged sites by incorporating hydrologic information from many sites in the neighborhood of a particular homogenous region (Chiang et al., 2002).

Hosking and Wallis (1997) developed an L-moment approach as a new approach for regional flood frequency analysis. L-moments have theoretical advantages over conventional moments, the ability to characterize a wider range of distribution, and the robustness to the presence of outliers in the data when estimated from a sample. These characteristics make L-moments suitable for flood frequency analysis, including distribution identification and parameter estimation. Details of L-moments can be found in Hosking and Wallis (1997). In brief, L-moments are defined as linear combinations of probability weighted moments (PWM). The sample L-moment ratios, t_r, are based on the sample L-moments and are defined as:

Table 2
Hydro-geomorphic and climatic characteristics of the study catchments.

Station	Area (km^2)	Basin Slope (%)	Compactness coefficient	Drainage density	Mean elevation (m)	River slope	Tc[a] (min)	MDP[b] (mm)	River length (km)	Bifurcation ration
Aroos	292.5	32.0	2.1	0.74	2337.7	3.8	58.4	38.5	24.5	4.4
Cheshme	57.3	29.9	1.8	0.98	2971.6	3.2	48.9	34.8	3.7	3.4
Dehrood	1080.0	38.6	1.9	0.87	2155.2	2.2	73.2	68.1	51.2	3.2
Hanjan	187.6	34.2	1.7	0.85	2784.9	2.4	56.4	48.3	23.6	3.7
Hossienabad	7714.4	12.4	2.2	0.85	2244.1	0.8	143.5	38.5	193.7	3.7
Kahnak	11847.0	12.4	2.5	0.91	1925.3	0.6	168.6	35.3	271.5	3.9
Kaldan	132.7	51.9	1.7	0.79	2420.3	4.7	45.5	37.7	21.4	3.5
Kenarueih	6716.9	12.4	2.4	0.90	2294.8	0.7	130.3	41.8	152.9	3.6
Meidan	335.8	34.2	1.8	0.87	2718.8	2.2	63.2	39.7	31.6	3.2
Narab	7244.4	12.4	2.3	0.89	2278.2	0.6	139.6	33.9	177.9	3.6
Polbaft	142.3	12.3	1.8	0.85	2680.9	1.6	64.5	33.7	20.2	3.8
Ramoon	33.7	44.1	1.9	0.57	2186.7	5.8	27.1	40.8	2.9	3.1
Soltani	702.5	12.4	2.1	0.90	2518.7	1.0	86.1	80.1	51.4	3.7
Tighsiah	37.5	28.7	1.4	0.86	1872.1	3.1	31.2	42.4	3.8	6.0
Zarrin	300.0	29.7	1.8	0.91	2095.4	2.8	48.2	50.58	23.5	3.1

[a] Tc: time of concentration.
[b] MDP: maximum daily precipitation.

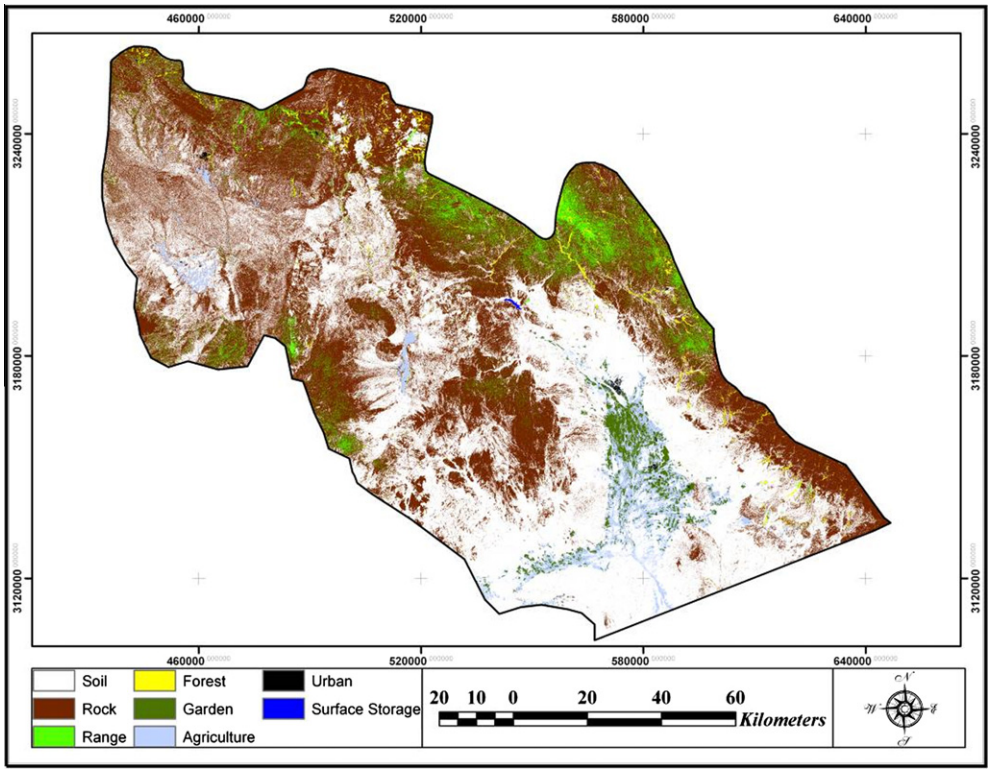

Fig. 3. Land use map of the Halilrud basin extracted from IRS-P6 satellite images.

Table 3
Land use attributes of the study catchments (the unit is hectare in all of the land use classes).

Station	Bare lands	Rock	Range	Forest	Gardens	Agriculture	Urban	Surface storage
Aroos	3715.0	19865.1	5040.4	633.4	–	–	0.2	–
Dehrood	10884.5	63330.9	28507.5	4741.5	213.7	269.4	57.4	–
Hanjan	4045.3	13665.2	405.2	566.4	–	–	78.3	0.4
Hossienabad	311882.0	402369.0	35601.0	9660.3	511.4	10022.2	1075.5	346.4
Kahnak	499865.0	535222.0	67489.7	16493.0	20817.6	42132.4	2360.9	359.3
Kaldan	942.4	7023.9	4217.7	1002.3	41.1	50.0	1.3	–
Kenarueih	277365.0	346108.0	27848.4	8924.1	445.3	9944.9	1074.9	1.5
Meidan	5499.6	24384.9	2302.6	1177.1	–	–	221.3	0.5
Narab	290650.0	378673.0	33842.0	9621.6	445.3	9944.9	1075.1	210.6
Pol-baft	1602.9	11346.8	1005.0	254.0	–	–	23.0	–
Ramoon	612.8	2485.6	266.9	5.8	–	–	–	–
Soltani	25478.5	40784.1	2771.7	759.7	30.7	280.7	152.5	–
Tighsiah	275.2	5364.8	21.7	148.8	–	–	–	–
Zarrin	4379.0	17239.1	6528.6	1545.6	112.4	151.5	54.4	–

$$t_2 = \frac{l_2}{l_1} \quad t_3 = \frac{l_3}{l_2} \tag{1}$$

where t_2 is the sample of L-Coefficient of variation (LCv) and t_3 is the sample of L-Coefficient of Skewness (LCs). The L-moment ratios will be used for homogeneity analysis in the regional frequency analysis.

The degree of hydrologic homogeneity is very important for reliability of the RFFA. The formation of the homogenous regions includes two steps. In each step, a statistical test is used, i.e., a (i) discordancy test, and (ii) heterogeneity test (Hosking and Wallis, 1997).

3.1.1. Homogeneity and discordancy tests

Hosking and Wallis (1997) derived two statistics to test the homogeneity of a region. The first statistic is used as a discordancy measure. The discordancy measurement, D_i, is used to screen out unusual sites from the pooling group (i.e., the sites whose at-site sample L-moments are markedly different from those for the other sites). D_i is defined as follows:

$$D_i = \frac{1}{3}(u_i - \bar{u})^T S^{-1}(u_i - \bar{u}) \tag{2}$$

where u_i is the vector of L-moments, and LCv, LCs, and L-Coefficient of Kurtosis (LCk) are for a site i;

$$S = (N_s - 1)^{-1} \sum_{i=1}^{N_s} (u_i - \bar{u})(u_i - \bar{u})^T \tag{3}$$

$$\bar{u} = N_s^{-1} \sum_{i=1}^{N_s} u_i \tag{4}$$

and NS is the number of sites in the group. In general, a site is declared discordant if $D_i > 3$ (Hosking and Wallis, 1997).

Hosking and Wallis (1997) also suggested a statistic as a heterogeneity measure (H) to define regional homogeneity. For hetero-

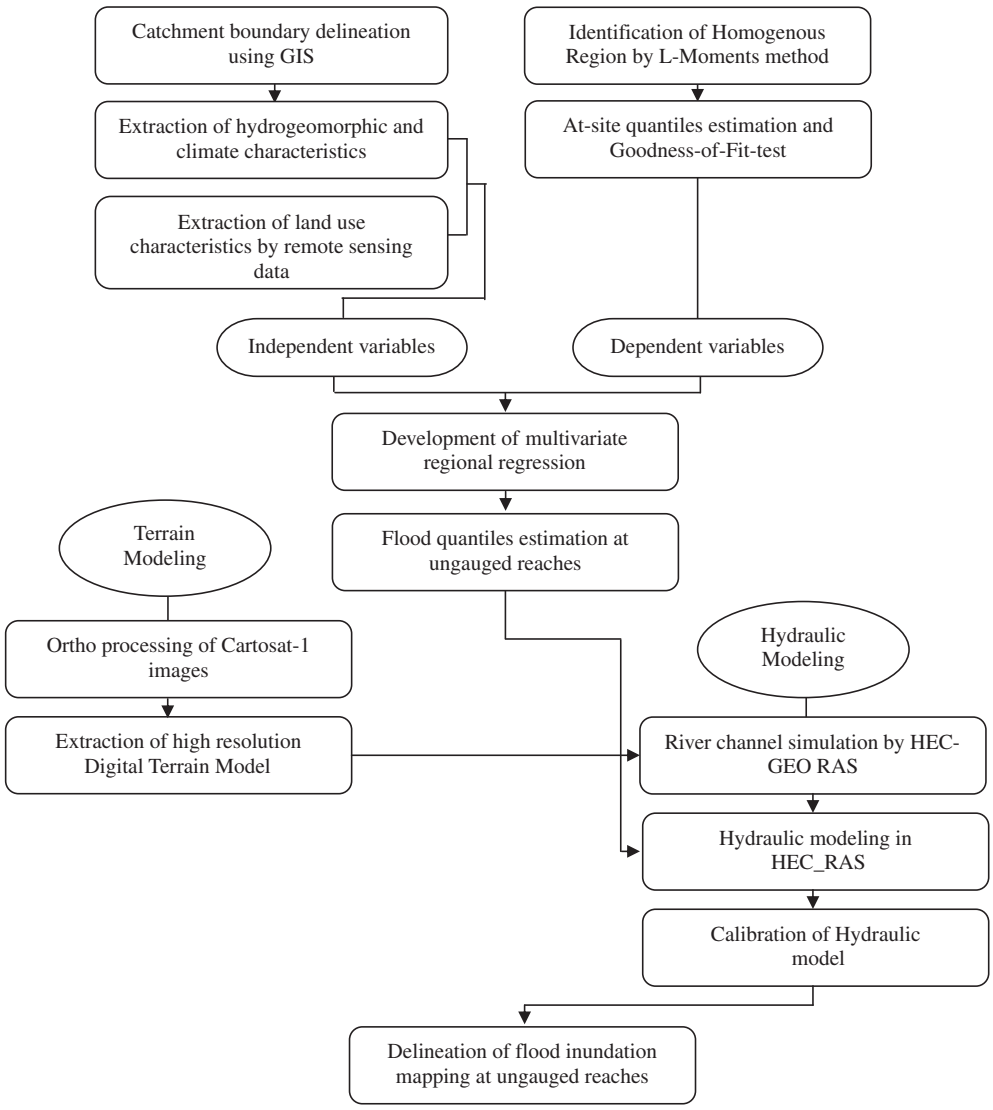

Fig. 4. Summarized procedure of the study.

geneity testing of sites, a four parameter kappa distribution is fitted to the regional data set generated by a series of 500 equivalent region data generated by numerical simulation. The test compares the variability of the statistics of an actual region to those of the simulated series (Hosking and Wallis, 1997).

There are three heterogeneity measurements (Hi): H_1, H_2 and H_3 associated with LCv scatter and the LCv–LCs and LCs–LCk relationship, respectively. These three measurements are calculated by the following equation:

$$H_i = (V_{obs} - \mu_V)/\sigma_V \tag{5}$$

where μ_V and σ_V are the mean and the standard deviation of Nsim values of V, Nsim is the number of simulation data, V_{obs}, is then calculated from the regional data and is based on the corresponding V-statistic, defined as follows:

$$V_1 = \sum_{i=1}^{N}\left(n_i\left(L - CV_i - \overline{LCV}\right)^2\right) \Big/ \sum_{i=1}^{N} n_i \tag{6a}$$

$$V_2 = \sum_{i=1}^{N}\left(n_i\left[\left(L - CV_i - \overline{LCV}\right)^2 + (\tau_{3i} - \overline{\tau})^2\right]^{1/2}\right) \Big/ \sum_{i=1}^{N} n_i \tag{6b}$$

$$V_3 = \sum_{i=1}^{N}\left(n_i\left[(\tau_{3i} - \overline{\tau_3})^2 + (\tau_{4_i} - \overline{\tau_4})^2\right]^{1/2}\right) \Big/ \sum_{i=1}^{N} n_i \tag{6c}$$

A region is acceptably homogenous if $H < 1$, is possibly heterogeneous if $1 \leqslant H < 2$, and definitely heterogeneous if $H \geqslant 2$ (Hosking and Wallis, 1997). Hosking and Wallis (1997) observed that the statistics H_2 and H_3 lack the power to discriminate between homogeneous and heterogeneous regions and that H_1 based on LCv had much better discriminating power. Therefore, the H_1 statistic is recommended as a principal indicator of heterogeneity (Hosking and Wallis, 1997).

3.1.2. Identification of the best-fit regional distribution

The important step in regional frequency analysis is to determine and to fit a parent distribution to flood series at sites in the homogeneous regions. This issue is very important for large return periods, because flood quantile estimates are affected by the type of distribution. The goodness-of-fit measurement is used to identify the regional parent distribution. This measurement, Z^{Dist}, judges the difference between sample L-Kurtosis and population L-Kurtosis for the fitted distribution (Hosking and Wallis, 1997).

The goodness-of-fit measure is defined as:

$$Z^{Dist} = (\tau_4^{Dist} - \bar{\tau}_4 + \beta_4)/\sigma_4 \quad (7)$$

where "Dist" refers to the candidate distribution, $\bar{\tau}_4$ is the average L-Kurtosis value computed from the data of a given region, β_4 is the bias of the regional average sample L-Kurtosis, and τ_4^{Dist} is the average L-Kurtosis value computed from the simulation for a fitted distribution. The goodness-of-fit of candidate distribution is considered suitable at a confidence level of 90% if $|Z^{Dist}| \leqslant 1.64$.

The regional candidate distribution is selected by this approach. The next step will be a transfer to the ungauged sites.

3.1.3. Developing multivariate regional regression model

To delineate flood inundation boundaries at ungauged rivers of interest, we first need to estimate streamflow statistics at these sites by using regional regression models. Using an offset of gauged river sites, a multivariate linear regression method establishes a relationship between streamflow statistics as dependent variables, and hydro-geomorphic, climatic and land use characteristics as independent variables as shown in Fig. 4 (Chiang et al., 2002; Vogel et al., 1999). Multivariate linear regression models most often have the following form:

$$Q_T = k + \alpha_1 X_1 + \alpha_2 X_2 + \ldots + \alpha_p X_p \quad (8)$$

where Q_T is the flood magnitude in a specific return period and obtained by the regional flood frequency analysis, k is the regression intercept, and X_1, X_2,...,Xp are physiographic and climatic characteristics; and α_1, α_2,...,α_p are regression coefficients which should be estimated for each model. To develop a regional regression models for the Halilrud basin, a stepwise regression procedure was employed using at 5% significance level on the entering variables (Kroll et al., 2004; Modarres and Sarhadi, 2010). To check the accuracy of the models, the residuals are tested to be normally distributed and independent. One major limit in multivariate regression models is that a high correlation (multicollinearity) usually exists among the explanatory variables in the regression models. Multicollinearity can cause a regression estimator to be inflated and to be correlated with errors, which can produce inaccuracies in subsequent hypothesis tests regarding parameter significance (Kroll et al., 2004). In order to avoid this situation, Variance Inflation Factor (VIF), which indicates the possible presence of the multicollinieatity, was estimated for the models (Hirsch et al., 1992). The VIF is a function of the coefficient of determination (R^2) obtained by regression; each individual explanatory variable acts against all the other explanatory variables. If VIF (VIF = $1/(1-R^2)$) associated with any regressor exceeds 4–5, we would suspect that multicollinearity is present (Montgomery et al., 2004).

3.2. Delineation of the flood hazard mapping

After estimating flood flow quantiles in different predicted probabilistic scenarios by regional frequency analysis at ungauged rivers, the second step in the identification of the flood prone areas is to delineate flood inundation mappings. However, to increase the reliability of the flood hazard mapping at ungauged channels, the first step is to develop an approach that can generate more quantitative, spatially explicit information to provide better spatial understanding of the river channel.

3.2.1. Terrain modeling

A high resolution digital terrain model is needed to extract details of channel topography for a reliable hydraulic simulation. Moreover, flood inundation mapping, which needs the results of the hydraulic models to get water surface elevations at cross-sections, requires a river terrain model. Terrain elevations are then subtracted from simulated water surface elevations to get a spatial extent of flood inundation and flood depth (Noman et al., 2001). Therefore, high quality DTM can reveal channel geometry spatially and enhance the accuracy of a hydraulic model. A development of the new spatial tools to generate high-resolution digital surface models enables researchers to create a valid hydraulic model for floodplain inundation purposes. Many studies have considered HEC-RAS performance by high resolution DTM extracted from new data sources such as LiDAR and SAR data (Aggett and Wilson, 2009; Chen et al., 2009; Geerling et al., 2009; Martinez and Toan, 2007; Sanders, 2007; Schumann, 2007). Although these data sources facilitate topographic parameterization of hydraulic models and enhance model reliability, they are currently available only for a limited number of rivers. Since high resolution DTMs will improve the realism of the hydraulic model's predictive ability (Aggett and Wilson, 2009), and no one has attempted to study the generation of the digital surface models from high resolution optical satellite images, in this study, we introduce an approach to extract high resolution DTMs from stereo Cartosat-1 images along with the Rational Polynomial Coefficients (RPCs). High resolution DTMs extracted from Cartosat-1 images not only have the appropriate resolution for hydraulic simulation, but also are accessible for any rivers of interest worldwide. These features make Cartosat-1-based DTM preferable to DTMs extracted from LiDAR and SAR data.

Cartosat-1 carries two high-resolution imaging cameras: the afterward looking camera (Aft) and the foreword looking camera (For), both able to collect panchromatic images with a spatial ground resolution of 2.5 m. The 12,000 pixels, each with 7×7 microns, in the image plane are covering with the focal length of 1.98 m, a swath of 30 km with the forward view and 26.6 km with the backward view (Crespi et al., 2008; Gianinetto, 2009). These characteristics have made Cartosat-1 images a useful instrument for generating ortho-images and high-resolution digital surface models that can improve flow hydraulic simulation, especially in mountainous regions. To extract detailed DTM, we used ortho image processing. This process involves five steps: interior orientation, exterior orientation, tie point generation, triangulation, and model refining using ground control points.

Before hydraulic modeling, Cartosat-1 stereo data with RPC along with Ground Control Points (GCPs) are used to extract a high resolution digital terrain model. After the terrain modeling process, high quality GCPs are used to determine the quality of the products. These GCPs are acquired using Differential Global Positioning System (DGPS), which has an accuracy of less than 1 m. Totally 10 DGPs evenly distributed surveyed GCPs are transferred over overlap Cartosat-1 images. Four points are used as control points and the rest (6 points) are applied as check points. To control pair images adaptation, RMSE of the check points and control points were calculated, and the total image RMSE = 0.42 pixels was achieved. The extracted high resolution DTM from Cartosat-1 images is given for the study area in Fig. 5. High resolution DTM extracted from Cartosat-1 images is then utilized to characterize channel geometry for optimizing the hydraulic model. The GIS-based Geo RAS pre- and post-processors facilitate these optimization efforts after the generation and validation process. Cartosat-1 derived DTM with a horizontal spatial resolution of 2.5 m, which is considered as an optimal cell size in the generation of a cross-section (Aggett, 2005), is used to simulate the hydraulic condition of the study channels.

3.2.2. Hydraulic modeling

To delineate inundated areas, recent studies (Horritt and Bates, 2002; Noman et al., 2001; Patro et al., 2009) indicate that the current approaches are based on hydraulic simulation that intersects predicted water levels with a floodplain surface. Numerical models involve solving the governing equation for river flow and floodplains using computational algorithms. According to the discharge observations at upstream and downstream locations of the floodplain reach, numerical methods may consist of one-dimensional

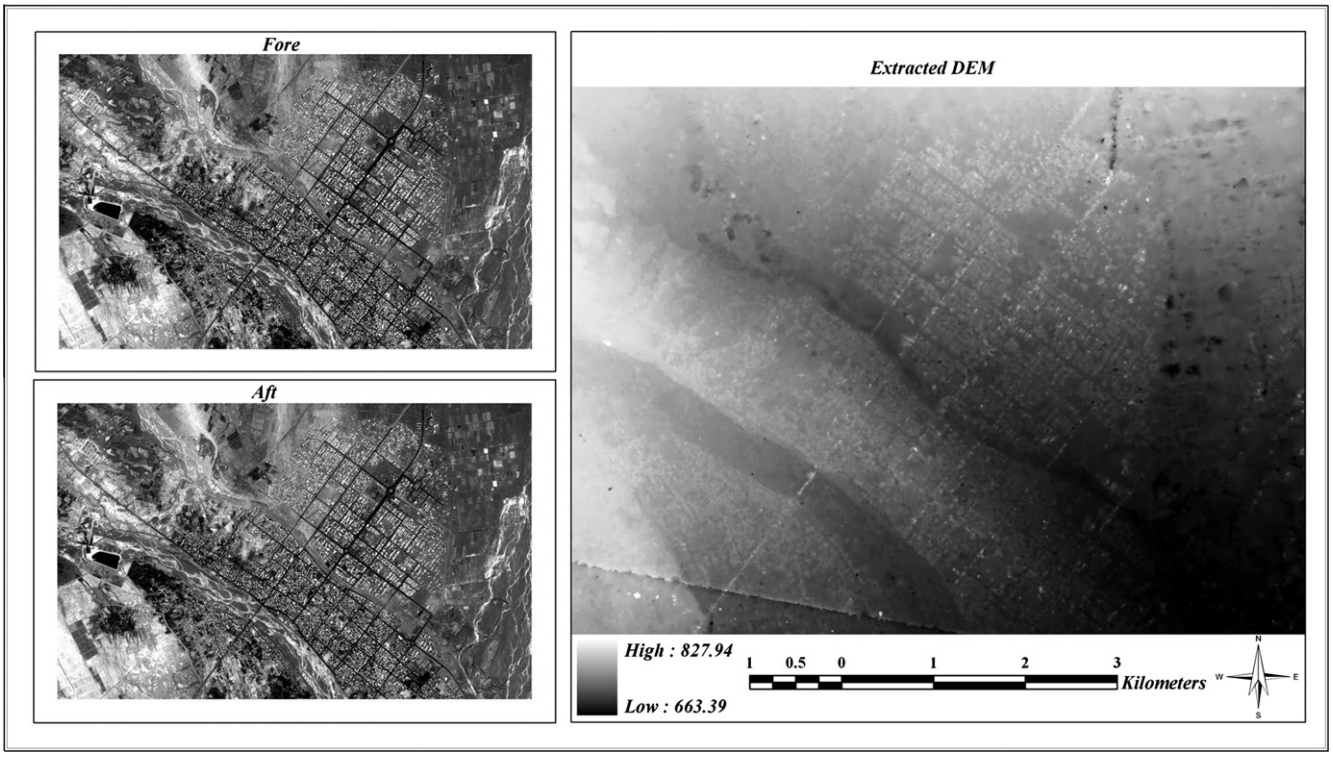

Fig. 5. High resolution DTM map extracted from pair stereo Cartosat-1 images (For and Aft).

or two-dimensional water surface models (Horritt and Bates, 2002; Nardi et al., 2006). As 2D modeling needs more complex and aggregate parameterization, a less complicated alternative 1D model, based on the St. Venant shallow water equations, is more popular among river engineers (Aggett and Wilson, 2009). HEC-RAS, a well-known 1D hydraulic model, can simulate one-dimensional steady and unsteady state flow conditions. In the steady state, HEC-RAS computes water surface elevation and velocity at successive cross-sections by solving continuity, energy, and flow resistance (e.g., Manning roughness) equations in a scheme called the standard step-backwater method. This model is able to modify channel geometry as well as flow data, and makes this opportunity for user to follow mixed flow regimes and flow distribution calculation via segmentation of the cross-sections geometric-based, hydraulic and roughness characteristics (Aggett and Wilson, 2009). Despite these advantages, results of the HEC-RAS models lead to a tabular and one-dimensional graphical output and a limitation in interoperation and analysis of the floodplain inundation. The recent development of HEC-GEO RAS, a GIS-based pre-and post-processing for parameterizing HEC-RAS with channel geometry, roughness and other hydraulic parameters, has considerably improved this situation (Aggett and Wilson, 2009; Maidment, 2002). Geo RAS can also provide a better visualization by importing predicted 2D water surfaces and velocity information to GIS. In the following sections we describe various hydraulic modeling steps performed by HEC-Geo RAS and HEC-RAS.

3.2.2.1. HEC-GEO RAS (GIS) pre-processing. In pre-processing, HEC-GEO RAS uses DTM and imagery to prepare the channel geometry required by HEC-RAS. The extraction of the spatial components for HEC-RAS input, specifically the stream centerline, riverbanks, levee and terrain cross-sections, is facilitated by pre-processing of HEC-GEO RAS. The location of the banks along the cross-sections extracted from DTM may not be very accurate in a flat area. Therefore, in these positions, each cross-section is manually checked and the banks are relocated, while cross-sections should not have the same position.

Since water surface profiles are found to be highly sensitive to cross-section spacing (Haile, 2005), the cross-section data are provided at intervals of less than 5 m. In addition to density, a cross-section's direction impresses flow calculations too. Depending on channel geometry changing, cross-section orientation should be changed. This is assuming that cross-section direction is as perpendicular to the stream centerline as possible. After digitizing very densely spaced cross-sections along three study reaches, they are then encoded with z values from the TIN surface. Finally pre-processing geometry data are exported to HEC-RAS.

3.2.2.2. Modeling in HEC-RAS. For hydraulic modeling in HEC-RAS, we need to have flow data, including flow rates; the flow change location, boundary conditions, topographic information in the form of a series of cross-sections, and the friction parameter in the form of Manning's n values across each cross section. To simulate water surface profiles of the ungauged reaches in the present study, we use flood quantiles at different return periods estimated by MRRMs as flow rates. For a steady state sub-critical simulation in this study, the slope of the reaches at the downstream end which was estimated from the Cartosat-based DEM at 0.0012 m m^{-1} was used as the model's initial boundary conditions. Although HEC-RAS allows for adjusting expansion and contraction coefficients, the default contraction and expansion coefficients of 0.1 and 0.3 were used (Brunner, 2006). For topographic information, an approach that employs high resolution Cartosat-based DTM (mentioned in Section 3.2.1) was used to derive characteristics of the channel geometry and morphology, including the channel cross-sectional area, gradient, wetted width, and the appropriate number of cross-sections.

All the cross-section's characteristics simulated in HEC-GEO RAS are imported into the HEC-RAS except Manning's roughness coefficient (n) values. Because of its sensitive role in hydraulic

simulation, the roughness coefficients is selected based on field assessment of the type and size of the bed, banks and over-bank material of the channel to make an initial base n value. This base value is corrected according to five factors of the channel characteristics including cross-section irregularity, channel variation, effect of obstruction, channel vegetation and degree of meandering (Coon, 1998). Each value of these factors is then added to the base n value, and the final Manning coefficient is formed for each cross-section. Moreover, geometry features and Manning's roughness coefficients (n) are developed and refined in a fully spatial setting for real visualization in the HEC-GEO RAS environment.

Suggested by HEC-RAS user's manual (U.S. Army Crops of Engineers, 2003), the HEC-RAS model needs to be validated using measured or remotely sensed data. As there is not any close gauged site in the study reaches, we used historical information of Jiroft city's February 1993 flash flood event to calibrate the HEC-RAS model. A set of estimated flood data during the high magnitude flood events was also used to validate the model.

To evaluate performance of the model, three quantitive indices, the inundation area, average inundation width, and the F statistic are used for the comparison of inundation maps (Bates and De Roo, 2000; Horritt and Bates, 2002).

$$F = \left(\frac{A_{op}}{A_o + A_p - A_{op}}\right) \times 100 \quad (9)$$

where A_o is the observed area of inundation, A_p is the predicted area of inundation, and A_{op} is area that is both observed and predicted as inundated. The F statistic varies between 100 when observed and predicted areas coincide perfectly, and 0 when no overlap between predicted and observed areas exists.

Moreover, to validate the terrain information extracted from Cartosat-1 based DTM, at least 2 cross-sections in each reach were selected as representative and compared with the same cross-section obtained via field surveying. This comparison provided a real base to validate water surface heights in the channel extracted from high resolution DTM of Cartosat-1. Following validation, the model was adjusted and run for flood quantiles in different probabilistic return periods. Free water surfaces and predicted cross-sectional inundations were then exported to HEC-GEO RAS for post-processing to improve visualization of the flood hazard mapping.

3.2.2.3. HEC-GEO RAS (GIS) post-processing. HEC-GEO RAS is able to import hydraulic modeling results into the GIS, where the intersection between the computed water level and the cross-sections enables the graphical geo-representation of the flooded areas to be made over the digital terrain model. Post-processing step involves generation of the different themes, including water surface profiles developed by HEC-RAS in TIN format. These TINs are then compared to the terrain TIN to define flooded areas. In order to perform this comparison, both the terrain and the water surface TINs are converted into GRID surfaces. The GRIDs are then compared, and flooded areas will be defined for those cells where the water surface is higher than the terrain elevation. After simulation of the hydraulic model for the historical flood events and flood quantiles in different return periods in HEC-RAS, all simulated water surfaces were imported into HEC-GEO RAS, and the visualization process of the flood inundations was performed by post-processing analysis.

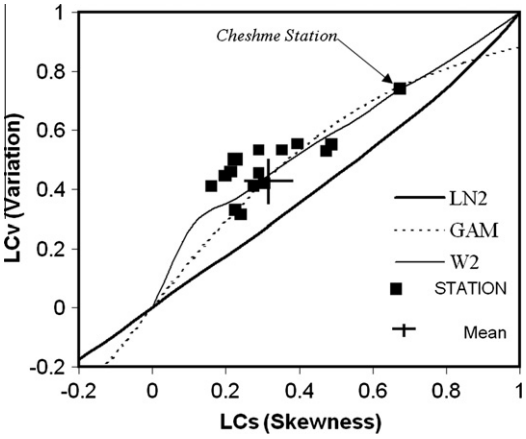

Fig. 7. LC_V–LCs moment ratio diagram for all stations.

4. Results and discussion

4.1. Regional flood frequency analysis

4.1.1. Homogeneity and discordancy tests

The heterogeneity of the annual maximum flows in the study region was tested using measures described in the methodology section. The L-Moment Ratio Diagrams (LMRDs) of the flood

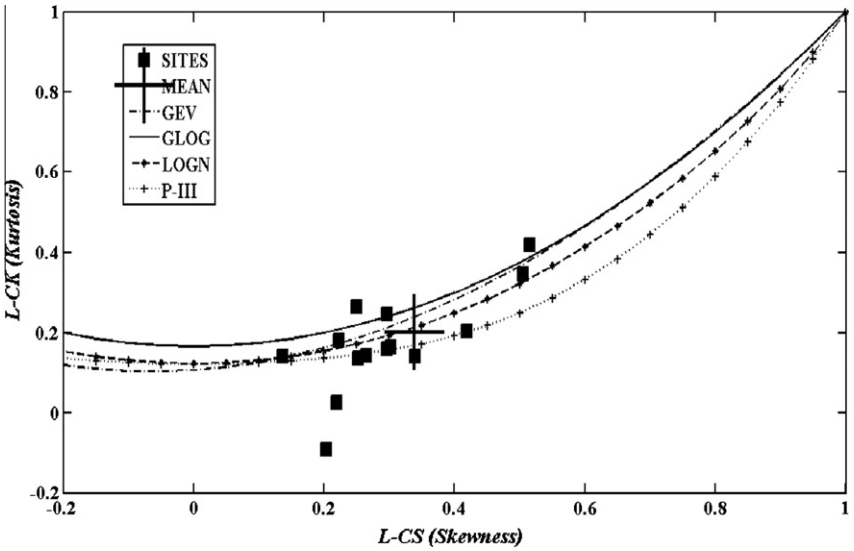

Fig. 6. LCs–LCk moment ratio diagram for all stations.

Table 4
L-moments statistics of the flood series in the study stations.

Station name	Sample size (year)	LCv	LCs	LCk	D
Aroos	14	0.31	0.25	0.23	1.17
Cheshme	20	0.76	0.67	0.45	3.03[a]
Dehrood	34	0.50	0.51	0.38	1.09
Hanjan	17	0.53	0.22	−0.01	1.97
Hossienabad	35	0.56	0.50	0.32	0.83
Kahnak	21	0.45	0.26	0.14	0.25
Kaldan	20	0.44	0.23	0.06	0.64
Kenarueih	13	0.40	0.26	0.15	0.37
Meidan	21	0.45	0.29	0.16	0.04
Narab	14	0.30	0.22	0.18	1.14
Polbaft	26	0.45	0.30	0.16	0.05
Ramoon	14	0.41	0.17	0.13	2.11
Soltani	36	0.53	0.34	0.14	0.33
Tighsiah	20	0.56	0.40	0.19	0.48
Zarrin	22	0.42	0.29	0.22	0.48

Table 5
Results of the homogeneity measure before and after removing discordant station.

Regions	Number of stations	Included stations	H_1	H_2	H_3
Halil basin	15	15	0.44	−0.05	−0.61
	15	14	0.19[a]	−0.25	−0.80

[a] Show homogeneity measure (H_1) after removing the discordant station.

Table 6
The goodness-of-fit-test measure (Z^{Dist}) for the homogeneous region.

Region	GLOG	GEV	LN3	P3	GPAR
Halil basin	1.74	0.79	0.01[a]	−1.32	−1.23

[a] The distribution accepted as a regional distribution.

magnitudes are illustrated in Figs. 6 and 7, and the values of L-zxmoments are also given in Table 4. These diagrams can be used to identify the sites which may have different statistical characteristics.

Despite comparative scattering of data points (Fig. 6, which is due to flood magnitudes in different catchments), except one station in Fig. 7 (with LCv: 0.761 and LCs: 0.679) a degree of homogeneity can be identified from LMRDs. In spite of this, heterogeneity measures were used to check the homogeneity and the existence of the discordant stations in the study region. As shown in Table 4, based on the critical value of D_i, Cheshme station is considered a discordant station. By removing this station from the dataset, homogeneity of the rest stations was then investigated by H statistics. The result of this test is presented in Table 5. According to H_1 measurement, which is reported to be discriminatory and more powerful than either H_2 or H_3 (Hosking and Wallis, 1997), the study area is acceptably homogenous.

4.1.2. Quantile estimation and goodness-of-fit-test

Quantile estimation is the main task in flood frequency analysis. For selection of the best regional frequency distribution function, the goodness-of fit-test measure, Z^{Dist}, was calculated using the FORTRAN computer program developed by Hosking (1991), and its results are presented in Table 6. It is clear that any distribution function can be selected as a regional distribution function according to the criteria of $|Z_{Dist}| \leqslant 1.64$, but the 3-parameter Log normal distribution function is more acceptable than other functions due to the smaller value of $|Z^{Dist}|$.

At-site frequency analysis for each gauging station was then carried out, and the LN3 distribution function was used to estimate probabilistic flood quantiles at each site. Table 7 presents flood quantile estimations of each single site in different return periods. These estimated quantiles are then used as dependent variables in the formation of regional flood regression models.

4.2. Flood quantiles estimation at ungaged sites

4.2.1. Development of regional flood regression models

After delineation of a homogenous region and at-site flood quantile estimation to estimate flood quantiles at ungauged sites, a stepwise multiple regression was used to develop the relationship between at-site flood quantiles (as dependent variables) and hydro-geomorphic and land use characteristics (as independent variables). The best multiple linear regression models, with a 1% significance level on the entering variables for the Halilrud basin, are presented in Table 8. The performances of the regional regression models in different return periods are given in Fig. 8 in the term of R^2. The validation of the models was also investigated by normality and independency tests of the residuals. The results of VIF are also given in Table 8 and used to determine whether a multicollinearity exists between independent variables. As shown in this table, no multicollinearity exists in the regression models.

The regional regression models indicate that physio-hydrological and land use characteristics are the major factors controlling frequent floods with low return periods. Shallow soils underlain by less-permeable bedrock covering most areas of the basin may contribute to flood generation either by producing saturation-excess overland flow or by exfiltrating directly into rivers. On the other hand, vegetation cover controls the infiltration and increases the soil moisture retention capacity. It is generally accepted that changes in land-use (e.g. residential development and road-construction, deforestation, etc.) and vegetation cover contribute to an increased frequency and severity of flood generation (Wahren et al., 2009).

Table 7
Estimated at-Site flood quantiles by the regional distribution function (LN3) in different return periods.

SITES	Aroos	Dehrood	Hanjan	Hosseinabad	Kahnak	Kaldan	Kenaruieh	Meidan	Narab	Pol-baft	Ramoon	Soltani	Tigh-siah	Zarrin
Return period (year)	Best Regional Distribution (LN3)													
2	84.4	20.2	67.7	52.8	182.4	18.2	177.5	74.41	107.4	10.5	17.5	32.8	9.8	18.8
5	132.6	35.2	123.2	205.2	323.5	31.1	316.8	164.5	167.8	24.4	30.5	59.3	25.8	35.2
10	184.8	44.6	135.4	367.4	423.9	37.7	381.6	181.4	178.4	32.7	39.5	95.7	42.7	55.7
20	236.3	58.4	165.7	533.6	477.2	45.6	456.3	209.7	187.5	38.5	45.5	109.4	68.5	67.8
50	312.7	99.4	173.8	1189.6	623.0	52.3	519.2	227.5	218.8	46.5	51.7	142.3	115.3	88.8
100	374.8	118.3	197.7	1482.2	681.4	62.5	542.7	244.5	230.8	50.5	58.7	153.8	157.1	110.4
200	452.2	145.6	215.7	1978.0	755.3	68.9	582.7	273.1	242.9	54.5	63.5	167.8	213.6	136.5
500	512.6	189.5	228.5	2381.1	875.5	78.9	642.8	291.4	266.4	59.6	67.2	188.5	287.8	164.1
1000	5832.1	251.7	247.5	3751.8	967.9	89.9	678.2	324.4	283.1	63.2	73.5	195.2	385.7	186.2

Table 8
Multivariate linear regression models for flood quantiles in different return periods.

Return period (year)	Best Regression Model	R^2	VIF	*P*-values of KS test
2	$Q_2 = 36.44 + 82.36CR6 - 0.323SS$	0.824	2.9	0.563
5	$Q_5 = 53.99 + 146.9CR6 - 0.004S + 7.67CR3$	0.881	1.25	0.674
10	$Q_{10} = 67.56 + 0.012Rg - 0.011Ag$	0.839	1.53	0.853
20	$Q_{20} = 76.78 + 0.026Rg - 0.002RL4 - 1.02SS$	0.874	1.45	0.884
50	$Q_{50} = 130.38 + 0.029Rg - 0.003RL4$	0.835	1.03	0.753
100	$Q_{100} = 156.67 + 0.041Rg - 0.004RL4$	0.823	1.02	0.805
200	$Q_{200} = -1605.5 + 0.06(Rg) - 0.006(RL.4) + 0.69(M.e)$	0.816	1.06	0.946
500	$\ln(Q_{500}) = 47.7 + 14.4 \ln(Max.e) + 7.01 \ln(Dd)$	0.751	1.04	0.565
1000	$\ln(Q_{1000}) = -49.7 + 14.9 \ln(Max.e) + 7.6 \ln(Dd)$	0.743	1.03	0.62

S: Soil.
Rg: Range lands.
Ag: Agriculture lands.
CR_n: Total number of streams with specific rank.
RL_n: River length with rank of *n*.
S.S: Surface storage.
M.e: Mean of elevation.
Max.e: Maximum of elevation.
Dd: Drainage density.

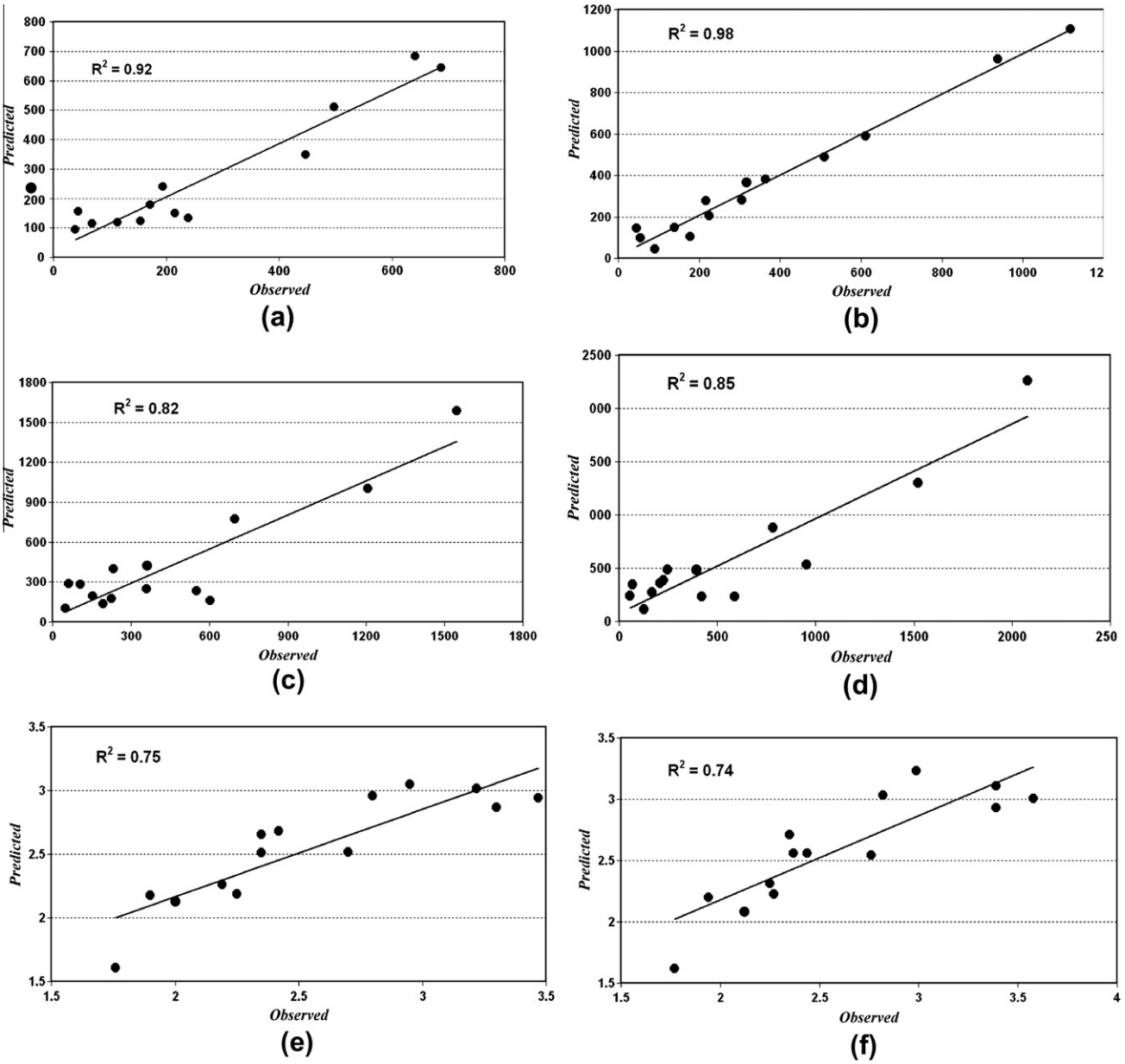

Fig. 8. Comparison of the observed and the estimated flood quantiles by regression method in different return periods (Tr), (a) Tr = 20, (b) Tr = 50, (c) Tr = 100, (d) Tr = 200, (e) Tr = 500, (f) Tr = 1000.

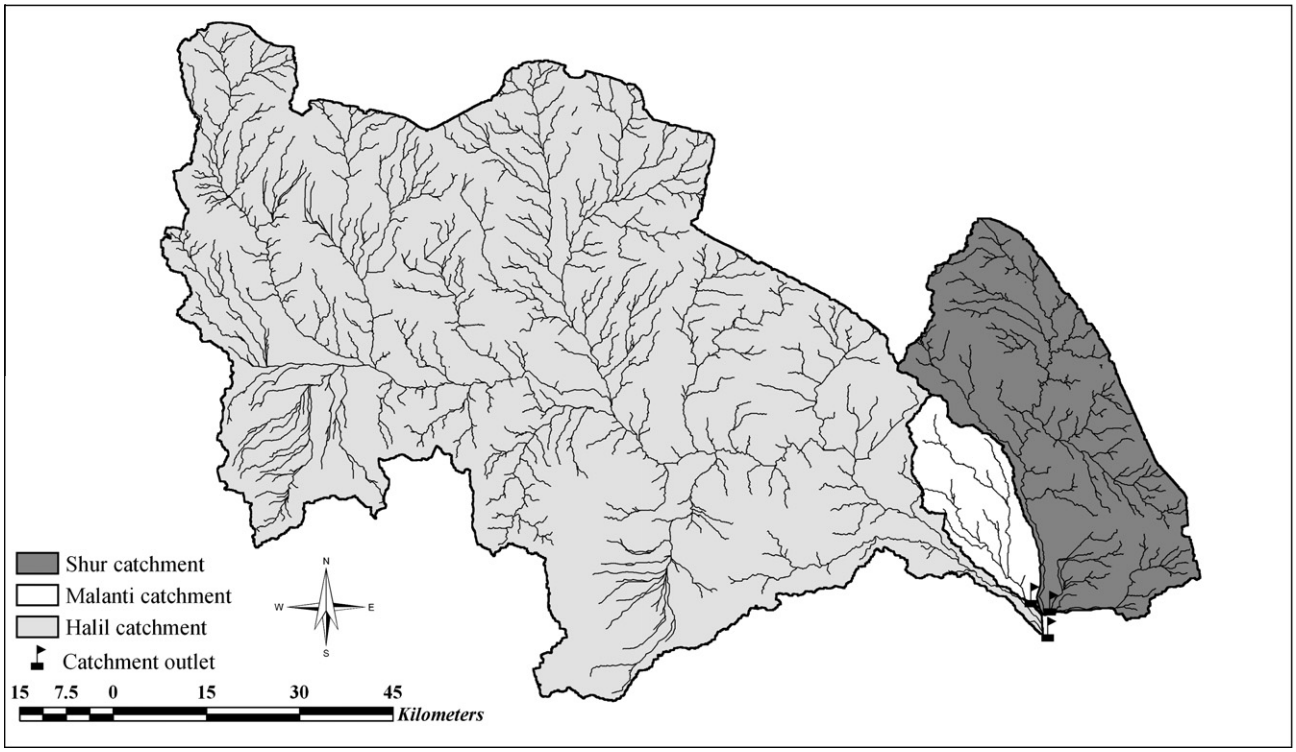

Fig. 9. Location of the outlet points and catchments of the three ungauged reaches.

Table 9
Estimated flood quantiles at the outlet of the ungauged reaches in different return periods at downward of Jiroft city.

Reach	Basin area (ha)	Return period								
		Q_2	Q_5	Q_{10}	Q_{20}	Q_{50}	Q_{100}	Q_{200}	Q_{500}	Q_{1000}
Halil	785022.8	92.7	265.2	435.8	667.7	1099.5	1640.7	2008.0	2907.1	4028.1
Shour	148035.7	23.7	42.8	55.6	75.8	123.8	157.2	202.1	267.9	389.3
Malanti	39014.3	17.6	30.9	41.2	50.4	64.8	76.6	88.4	101.0	124.5

Table 10
Goodness of fit between observed inundation extent and that predicated by HEC-RAS hydraulic model (Note: F statistic is computed using Eq. (9)).

Performance	Date	Observed	Predicted		
			Width (m)	Area (km^2)	F (%)
Calibration	5 February 1993	3800	496.6	73.15	89.82
Validation	2 March 1972	1082	331.8	46.57	85.48
	26 February 1971	820	286.7	32.90	83.76
	9 February 1995	610	275.2	31.12	76.31

Although there is no valid information on land use change in arid and semi-arid regions of Iran, changes in the vegetation cover, usually rangelands and forest areas to agricultural land use which can be assumed to be the main reason in changes of the soil hydraulic properties (decreasing soil infiltration and water retention capacity) lead to an increasing surface runoff and the probability of flash flood occurrences in arid and semi-arid regions of Iran (Sarhadi and Modarres, 2011).

The models also show that physical characteristics and severe topography are dominant factors having a key role in the flood generation process in higher return periods (infrequent floods). A catchment's topography characteristics that form hydraulic head differences cause surface water to flow to the main channel, and high drainage density affects the flow volume and velocity, and leads to flashy hydrographs with a steep falling limb (Rodriguez-Iturbe and Rinaldo, 1997). Since physiographic and geomorphic characteristics are not manageable, soil conservation and proper land use management are considered to be the most important practices to decrease flood magnitudes in the Halilrud basin.

It should also be noted that the absence of the MDP in the regression models may be related to the resolution of precipitation data. As time of concentration plays a dominant role in the generation of extreme floods with the short period rainfall, it seems that hourly resolution would be a better climate indicator than the daily precipitation variable. Because of the short concentration time of the study drainage catchments (shown in Table 2) which are between 27.1 and 168.6 min, the maximum daily precipitation cannot influence the flash flood generation process. On the other hand, less-permeable rock formations underlying the shallow topsoil covering most catchments of the basin accompanied with steep mountains slopes give

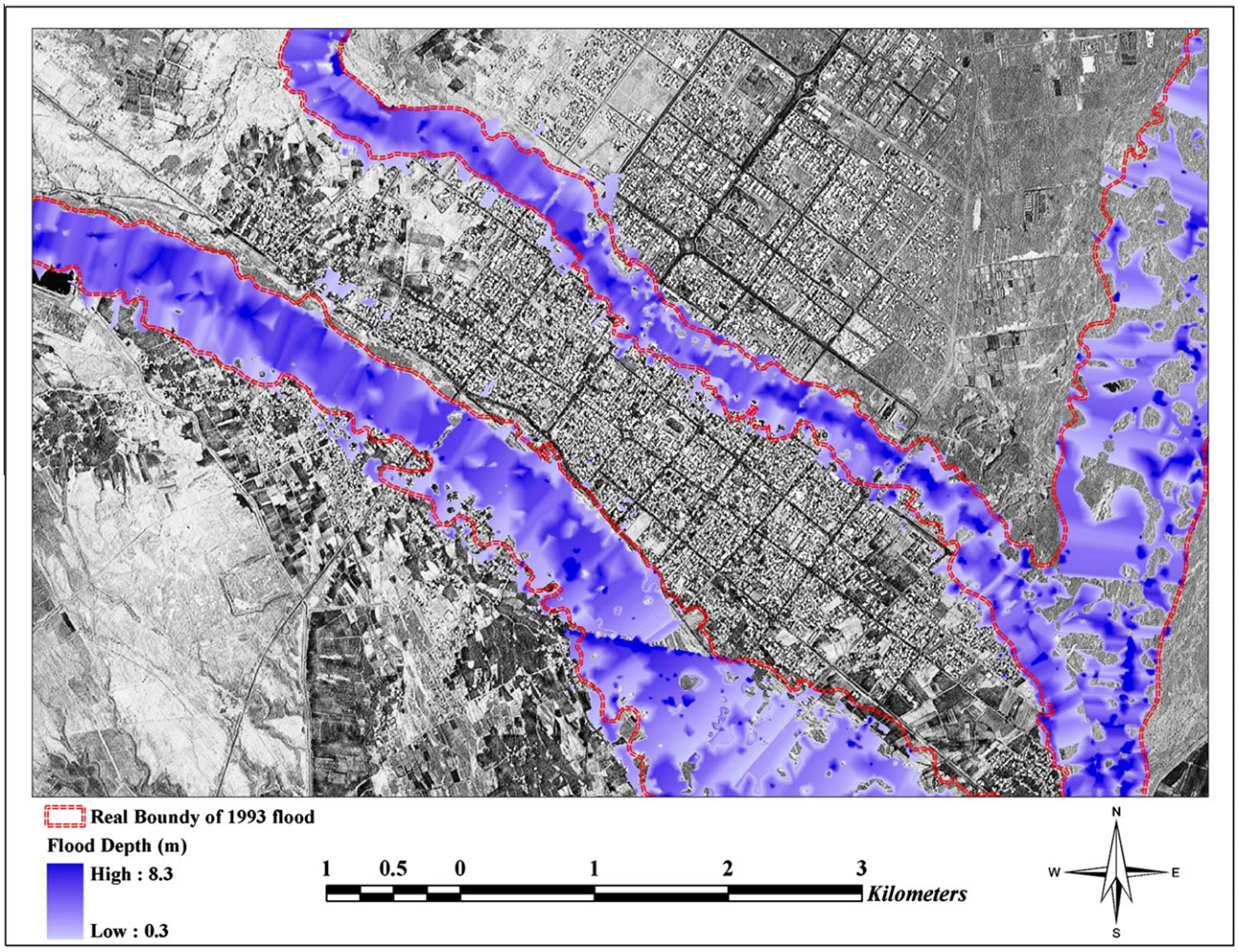

Fig. 10. Simulated 1993 historical flood event at the vicinity of Jiroft city.

Table 11
Area of the land use classes (ha) affected by floods in different probabilistic scenarios.

Land-use	Reach	Q_{20}	Q_{50}	Q_{100}	Q_{200}	Q_{500}	Q_{1000}
Road	Halil	2.85	8.83	11.23	20.45	29.45	35.65
	Shour	0.21	3.81	5.42	9.62	13.11	15.52
	Malanti	–	0.21	0.98	1.95	3.01	3.8
Residential area	Halil	2.05	15.31	42.24	53.24	67.76	87.12
	Shour	–	–	–	12.44	18.25	31.25
	Malanti	–	–	4.58	9.51	16.34	24.2
Green space	Halil	4.2	9.15	18.35	27.25	46.61	57.65
	Shour	–	0.2	0.86	1.45	6.78	9.54
	Malanti	–	–	1.10	3.14	8.82	14.57
Garden	Halil	45.6	168.52	210.08	400.16	672.76	813.12
	Shour	22.3	68.25	106.25	206.25	231.25	300.1
	Malanti	–	–	–	9.38	23.05	32.1
Agriculture	Halil	26.2	62.22	143.64	192.04	303.36	414.68
	Shour	39.74	73.52	175.0	223.75	356.25	425.2
	Malanti	–	–	1.26	3.68	8.52	14.52

rise to the surface soil to be saturated rapidly and facilitate excess runoff generation due to rapid response of the catchments to short and intense rainfall events. Therefore, because of special hydro-geomorphic characteristics of Halilrud basin and the stronger effects of the physio-hydrologic and geomorphic characteristics than the effect of precipitation factor, it can be deduced that the maximum 24 h rainfall (daily resolution) cannot be an effective factor on flash flood generation in the study area to appear in the regression model. Hence, in addition to MDP data, we recommend other precipitation data with hourly resolutions to be added to the database for performing MRRMs especially in arid and semi-arid regions.

However, since the information on heavy short-period rainfall data is not available for Halilrud basin to be included in regression models, we developed our MRRMs using the available variables. Nevertheless, it is needed to evaluate the above statement of the effect of heavy rainfall on flash flood in the next studies.

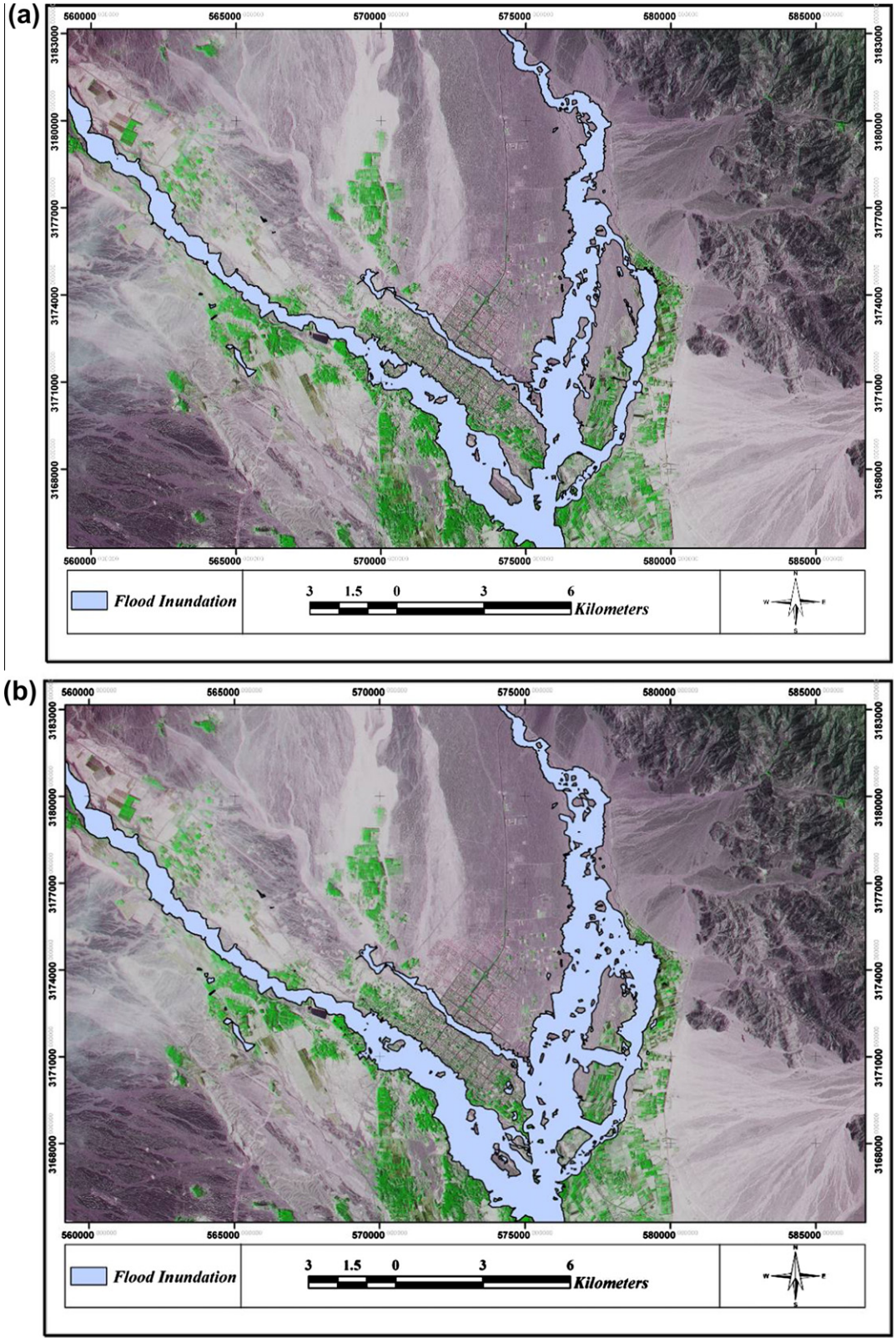

Fig. 11. Flood hazard inundation maps at ungauged reaches in different return periods (Tr), (a) Tr = 100, (b) Tr = 200, (c) Tr = 500, (d) Tr = 1000.

4.2.2. Flood quantiles estimation at ungauged reaches

After establishing regional models, to estimate flood quantiles at ungauged reaches, upward catchment characteristics of each specific point (as a catchment outlet) along a river are replaced on the regional flood models to transfer flood information from gauged sites to the interest point. To do this, in three ungauged reaches encircling Jiroft city, the outlet points must be first determined. As the investigation of the flood hazard inundation in Jiroft city is a principle purpose of this study, the junction of the three reaches down from the city was selected as the outlet of the

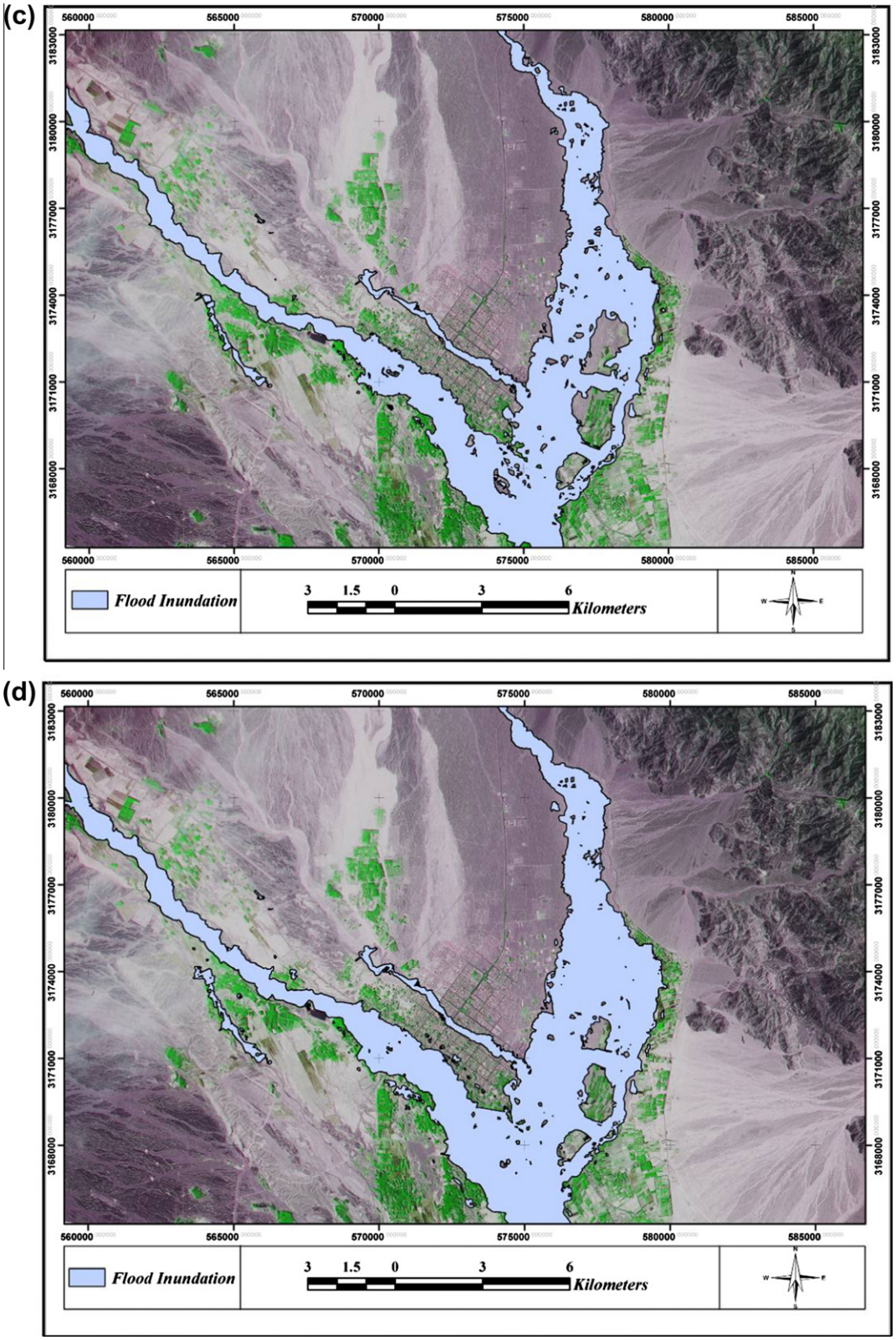

Fig. 11 (*continued*)

reaches. Fig. 9 shows the location of the selected outlets and the corresponding catchments of the ungauged reaches. After extraction of the related catchment boundaries and their independent parameters using HEC-GEO HMS, these parameters were replaced on the regional models, and flood quantiles in different return periods were estimated at the selected outlets. Estimated flood quantiles for each reach are given in Table 9. These flood quantiles in different return periods are then used as various probabilistic

scenarios to simulate water surfaces in hydraulic modeling process, and to distinct areas that are affected by flood magnitudes under various scenarios.

4.3. Floodplain inundation mapping

HEC-Geo RAS was used to create geometry data for HEC-RAS using Cartosat-based DTM. Initially, 502 topographic cross-sections were created for three study reaches. The channel bed and over-bank boundaries were digitized to provide flexibility in the allocation of different surface roughness coefficients (Manning's n), based on size and shape of the bed materials (Barnes, 1967). Additional cross-sections were also interpolated in HEC-RAS for a better channel geomorphology defining. Totally, 562 cross-sections were created along three study reaches. The geometry was then imported into HEC-RAS. Optimal Manning's n coefficients, which were carried out for in-channel and over-bank cross-section slices based on field assessment and channel characteristics range from 0.022 to 0.045 for Halilrud reach, from 0.025 to 0.051 for Shur reach, and from 0.020 to 0.032 at Malanti reach. Generally, because of sedimentation, the surface roughness in the channels is less than for over-bank areas.

To calibrate the HEC-RAS model, we used the estimated discharge rate of the 1993 historical flood event and information of this catastrophe gathered by the Ministry of Power (Sarhadi, 2008) to simulate this historical flood inundation map. According to the frequency analysis (Table 9), the 1993 flood event is counted as an infrequent flood disaster with a return period of about 1000 years. By running the HEC-RAS model based on the estimated discharge of this flood (3800 m^3/s) at the downward junction point of the reaches, the flood inundation for this extreme event was simulated (Fig. 10). Since, during this catastrophe no satellite recorded any optical images from this region because of cloudy sky, the only evidence used for calibration was an inundation extent map provided by Ministry of Power staff, who traced the tide marks shortly after this event (this boundary is shown with a red dash line in Fig. 10) (Sarhadi, 2008). A comparison of model and observed results for the 1993 historical event is shown in Fig. 10, whilst the value of the F coefficient is given in Table 10. Fig. 10 and F value in Table 10 show that for peak flow in February 1993, the model does a coherent match at simulating the observed inundation extent, with only a very small amount of over-prediction in over-bank areas, due to changes of the surface roughness. Regardless of the accuracy of the Cartosat-based DTM (with resolution 2.5 m), such behavior is expected for U and V shaped rivers (such as the Halil and Shur rivers) when a raster based technique is used to simulate the spatial extent of flood inundation areas and flood depth by subtracting DTM from the water surface elevation.

After some corrections and refinements on over-bank cross-sections, model validation, which refers to the evaluation of the hydraulic model performance for predicting flood inundation, was done for a number of flood events with different estimated magnitudes at downward of Jiroft city. According to the F statistics in Table 10, except the 1995 flood event (as an frequent flood), both simulated infrequent flood events of 1971 and 1972 generally showed good correspondence to the observed data, and the model can still be regarded as relatively accurate. For the 1995 peak flow, because of differences between predicted and observed inundation, the F performance measure decreased to 76.31, presumably due to the simplified representation of shallow water hydraulics included in the HEC-RAS model or the fact that inundation extent at infrequent flood events may simply be easier to predict (Bates et al., 2006). However, the results indicate that the hydraulic model supports an excellent match for high discharge flood events causing considerable economic damage in the study area.

After validation, the HEC-RAS model was run to simulate the flood inundation mapping for flood quantiles in different probabilistic scenarios at the study ungauged reaches. Fig. 11 presents simulated flood inundation maps for high magnitude (low probability) floods. In these maps, inundated areas are co-displayed over a high resolution remote sensing image of IRS-P6 (fusioned with PAN band) to highlight spatial extension of the flood areas in various probabilistic conditions for a better understanding of the flooding hazard. Further, we are able to cross flooded areas with the extracted land use maps from these remotely sensed data to determine infrastructures and valuable land use classes affected by flooding.

Table 11 shows details of areas in each land-use class which are affected by different probabilistic scenarios at study reaches. The inundated land-use classes and infrastructures affected in low return periods flood events show a mis-utilization of the river banks, so that the irrigation fields located in low terraces along the Shur and Halil reaches are subject to flooding hazard of the high-frequent events. The flood damage potential is significantly increasing for the residential areas and valuable land-use classes in higher return periods. Due to the existence of most vulnerable infrastructures and areas with high population density along the both sides of the Halil and Malanti rivers, the highest risk and damages concern these rivers under simulated inundation condition for the high impact low frequency flood events. The results also reveal that low elevation agriculture and garden fields near the Shur river are exposed to flood hazard, and high magnitude flood occurrences could lead to significant damages to these properties.

Overall, in many cases due to the importance of the agriculture, rural and urban developments, flood hazards and probable damages are ignored along the study reaches. Therefore, special attention needs to be focused on land use planning and preparedness for the necessary activities in dealing with the adverse consequences of flooding in the Jiroft city area. Hence, flood inundation prediction under different probabilistic scenarios can help programmers as a basis for floodplain risk management and planning of agricultural, industrial and urban expansion to locate new developments in less risky areas along the ungauged rivers to minimize the social and economic impacts of flood hazard.

5. Summary and conclusion

In this paper, a comprehensive methodology for simulating flood hazard mapping at ungauged rivers is presented. This methodology links regional flood frequency analysis and hydraulic modeling to delineate flood inundation mapping. An L-moments approach as a reliable method was initially used to identify homogenous regions. To form regional multivariate regression models, the hydro-geomorphic and land use characteristics of the catchments (as independent variables) were extracted, and at-site flood quantiles in different return periods (as dependent variables) were estimated by RFFA. The performance and validation of the models were then checked by the related criteria. After delineation of the ungauged catchment boundaries, by replacing the relevant properties in regional flood models, flood quantiles in different return periods as one of the key elements in the flood inundation process were estimated for the outlets of the ungauged reaches. In hydraulic modeling, HEC-RAS model was coupled with high resolution DTM, extracted from satellite stereoscope images of Cartosat-1 to increase the reliability of the floodplain inundation predictions. Meanwhile the GIS-based pre- and post-processing facilitated accurate optimization of the geometry features and Manning's roughness coefficient (n) values for real visualization of the flood inundation areas. Validation of the HEC-RAS model was then confirmed according to the information of a historical flood with a return period of 1000 years. After this, the delineated flooded areas were simulated and crossed with the extracted land use mapping from high resolution IRS-P6 images to distinguish the infrastructures and valuable land uses which would be affected

in various probabilistic scenarios. Results show that Jiroft city has a critical situation from a flooding hazard point of view, so at each hazard level, some parts of different precious land uses areas are damaged by flooding. Therefore, it is essential that flood control structures be designed for this city and its rural areas. In this direction, flood inundation maps can help managers and decision makers to mitigate flooding damages and to establish flood warning systems.

Finally, we can use this proposed methodology to transfer hydrological information from gauged sites to ungauged catchments of interest and delineate flooding prone areas to decrease probable damage in areas with a high potential for flooding and which suffer from inadequate hydrologic information, especially in arid and semi-arid regions. The capability of the identification and prediction of the flood vulnerable areas at ungauged rivers is the major advantage of the proposed methodology presented in this study over those in previous studies and can help managers to cope with flooding hazards in optimum management and mitigation strategy definitions. Moreover, land use managers require the ability to identify various aspects of landscape vulnerability in probable flooding hazards. This methodology can help them to better understand the various level of protections needed to minimize and prevent damage from river systems; thus, the simulation of the river hydraulics and the visualization of the flood inundation in probable scenarios can be useful. As spatial GIS-based model predictions have until recently been limited by the unavailability of the appropriate DTMs, high resolution terrain modeling extracted from satellite stereo images (Cartosat-1), can develop detailed parameterization of the channel geometry and enhance the accuracy of hydraulic model outputs. This technology advances our ability to model the hydraulic processes in frequent and infrequent (dam-break) flood events. Therefore, these data sources are far more accurate and in fact quite useful in spatially detailed floodplain inundation studies.

References

Aggett, G., 2005. Applying Advanced Geospatial Data and Methods to Monitoring and Modeling Fluvial Processes. University of Southern California, Los Angeles, USA.

Aggett, G.R., Wilson, J.P., 2009. Creating and coupling a high-resolution DTM with a 1-D hydraulic model in GIS for scenario-based assessment of avulsion hazard in gravel-bed river. Geomorphology 113, 21–34.

Aronica, G., Hankin, B., Beven, K., 1998. Uncertainty and equifinality in calibrating distributed roughness coefficients in flood propagation model with limited data. Adv. Water Resour. 22 (4), 349–365.

Barnes, H.H., 1967. Roughness Characteristics of Natural Channels: U.S. Geological Survey Water-Supply Paper 1849, 213 p.

Bates, P.D., De Roo, A.P.J., 2000. A simple raster-based model for flood inundation simulation. J. Hydrol. 236 (1–2), 54–77.

Bates, P.D., Wilson, M.D., Horritt, M.S., Mason, D.C., Holden, N., Currie, A., 2006. Reach scale floodplain inundation dynamics observed using airborne synthetic aperture radar imagery: data analysis and modelling. J. Hydrol. 328 (1–2), 306–318.

Brunner, G.W., 2006. HEC-RAS, River Analysis System User's Manual, Version 4.0 Beta. U.S. Army Corps of Engineers, 420 pp.

Burn, D.H., 1990. Evaluation of regional flood frequency analysis with a region of influence approach. Water Resour. Res. 26 (10), 2257–2265.

Casas, A., Benito, G., Thorndycraft, V.R., Rico, M., 2006. The topographic data source of digital terrain models as a key element in the accuracy of hydraulic flood modelling. Earth Surf. Proc. Land. 31, 444–456.

Castellarin, A., Burn, D.H., Brath, A., 2008. Homogeneity testing: how homogeneous do heterogeneous cross-correlated regions seem? J. Hydrol. 360 (1–4), 67–76.

Chen, Y.D., Huang, G., Shao, Q., Xu, C.Y., 2006. Regional analysis of low flow using L-moments for Dongjiang basin, South China. Hydrol. Sci. J. 51, 1051–1064.

Chen, J., Hill, A.A., Urbano, L.D., 2009. A GIS-based model for urban flood inundation. J. Hydrol. 373, 184–192.

Chiang, S.M., Tsay, T.K., Nix, S.J., 2002. Hydrologic regionalization of watersheds. I: Methodology development. J. Water Resour. Plann. Manage. 128, 3–11.

Chokmani, K., Ouarda, T.B.M.J., 2004. Physiographical space-based kriging for regional flood frequency estimation at ungauged sites. Water Resour. Res. 40 (12). Art. No. W12514.

Chormanski, J., Okruszko, T., Ignar, S., Batelaan, O., Rebel, K.T., Wassen, M.J., 2011. Flood mapping with remote sensing and hydrochemistry: a new method to distinguish the origin of flood water during floods. Ecol. Eng. 37 (9), 1334–1349.

Cobby, D.M., Mason, D.C., 1999. Image processing of airborne scanning laser altimetry for improved river flood modelling. ISPRS J. Photogram. Rem. Sensing 56, 121–138.

Coon, W.F., 1998. Estimation of Roughness Coefficients for Natural Stream Channels with Vegetated Banks, Geological Survey (U.S.), New York (State). Dept. of Transportation.

Crespi, M., Fratarcangeli, F., Giannone, F., Colosimo, G., Pieralice, F., Jacobsen, K., 2008. Geometric Potential of Cartosat-1 Stereo Imagery, The International Archives of the Photogrammetry, Remote Sensing and Spatial Information Sciences, pp. 1323–1330.

Dalrymple, T., 1960. Flood Frequency Analysis, Water Supply Paper 1543_a. US Geographical Survey, Reston, VA.

ESRI, 1990. Understanding GIS: The ArcInfo Method. ESRI Press, Redlands, Calif., 400 pp.

Finlayson, D.P., Montgomery, D.R., 2004. Modeling large scale fluvial erosion in geographic information system. Geomorphology 53, 147–164.

Geerling, G.W., Vreeken-Buijs, M.J., Jesse, P., Ragas, A.M.J., Smits, A.J., 2009. Mapping river floodplain ecotopes by segmentation of spectral (CASI) and structural (LiDAR) remote sensing. River Res. Appl. 25, 795–813.

Gianinetto, M., 2009. Evaluation of cartosat-1 multi-scale digital surface modelling over France. Sensors 9, 3269–3288.

Gomes Pereira, L., Wicherson, R., 1999. Suitability laser data for deriving geographical information: a case study in the context of management of fluvial zones. ISPRS J. Photogram. Rem. Sensing 54 (2–3), 105–114.

Goswami, M., O'Connor, K.M., Bhattarai, K.P., 2006. Development of regionalisation procedures using a multi-midel approach for flow simulation in an ungauged catchment. J. Hydrol. 333, 517–531.

GREHYS, 1996. Inter-comparison of regional flood frequency procedures for Canadian rivers. J. Hydrol. 186 (1–4), 85–103.

Haile, A., 2005. Integrating Hydrodynamic Models and High Resolution DEM (LIDAR) for Flood Modeling. M.Sc. Thesis, ITC, Enschede, the Netherlands.

Hirsch, R.M., Helsel, D.R., Cohn, T.A., Gilroy, E.J., 1992. Statistical analysis oh hydrological data. In: Maidment, D.A. (Ed.), Handbook of Hydrology. McGraw-Hill, New York, pp. 17.1–17.55.

Horritt, M.S., Bates, P.D., 2001. Predicting floodplain inundation; rastered-based modelling versus the finite-element approach. Hydrol. Process. 15 (5), 825–842.

Horritt, M.S., Bates, P.D., 2002. Evaluation of 1D and 2D numerical models for predicting river flood inundation. J. Hydrol. 268 (1–4), 87–99.

Hosking, J.R.M., 1991. Fortran Routines for Use with the Method of L-moments, Version 2, Res. Rep. RC 17097. IBM Research Division, York Town Heights, NY.

Hosking, J.R.M., Wallis, J.R., 1993. Some statistical useful in regional frequency analysis. Water Resour. Res. 29 (2), 271–281.

Hosking, J.R.M., Wallis, J.R., 1997. Regional Frequency Analysis an Approach Based on L-Moment. Cambridge University.

Jian, G.L., Mason, P.J., 2009. Essential Image Processing and GIS for Remote Sensing. John Wiley & Sons Ltd..

Kroll, C.K., Vogel, R.M., 2002. Probability Distribution of low streamflow series in the United States. J. Hydrol. Eng. 7 (2), 137–146.

Kroll, C., Luz, L., Allen, B., Vogel, R.M., 2004. Developing a watershed characteristics database to improve low streamflow prediction. J. Hydrol. Eng. 9 (2), 116–125.

Li, M., Shao, Q., Zhang, L., Chiew, F.H.S., 2010. A new regionalization approach and its application to predict flow duration curve in ungauged basins. J. Hydrol. 389 (1–2), 137–145.

Lu, L.H., Stedinger, J.R., 1992. Sampling variance of normalized GEV/PWM quantile estimators and a regional homogeneity test. J. Hydrol. 138 (1–2), 223–245.

Maidment, D. (Ed.), 2002. Arc Hydro: GIS for Water Resources. ESRI Press, Redlands, CA, 203pp.

Marche, C., Lessard, G., Elgharbi, B., 1990. Kriging technique for river flood representation. J. Hydraul. Res. 28 (5), 629–643.

Martinez, J.M., Toan, T.L., 2007. Mapping of flood dynamics and spatial distribution of vegetation in the Amazon floodplain using multitemporal SAR data. Remote Sens. Environ. 108, 209–223.

Merwade, V., Cook, A., Coonrod, J., 2008. GIS techniques for creating river terrain models for hydrodynamic modeling and flood inundation mapping. Environ. Model. Softw. 23 (10–11), 1300–1311.

Merz, R., Blöschl, G., 2005. Flood frequency regionalisation—spatial proximity vs. catchment attributes. J. Hydrol. 302 (1–4), 283–306.

Modarres, R., 2008. Regional frequency distribution type of low flow in north of Iran by L-moments. Water Resour. Manag. 22, 823–841.

Modarres, R., Sarhadi, A., 2010. Frequency distribution of extreme hydrologic drought of Southeastern semi-arid region Iran. J. Hydrol. Eng. 15, 255–264.

Montgomery, D.C., Runger, G.C., Hubele, N.F., 2004. Engineering Statistics. Wiley Publications.

Nardi, F., Vivoni, E.R., Grimaldi, S., 2006. Investigating a floodplain scaling relation using a hydrogeomorphic delineation method. Water Resour. Res. 42, W09409. http://dx.doi.org/10.1029/2005WR004155.

Noman, N.S., Nelson, E.J., Zundel, A.K., 2001. Review of automated floodplain delineation from digital terrain models. J. Water Resour. Plann. Manag. 127 (6), 394–402.

O'Callaghan, J.F., Mark, D.M., 1984. The extraction of drainage networks from digital elevation data. Comput. Vis., Graph., Image Process. 28, 323–344.

Ouarda, T.B.M.J., Girard, C., Cavadias, G., Bobée, B., 2001. Regional flood frequency estimation with canonical correlation analysis. J. Hydrol. 254 (1–4), 157–173.

Ouarda, T., Cunderlik, J., St-Hilaire, A., Barbet, M., Bruneau, P., Bobée, B., 2006. Data-based comparison of seasonality-based regional flood frequency methods. J. Hydrol. 330, 329–339.

Pandey, G.R., Nguyen, V.T.V., 1999. A comparative study of regression based methods in regional flood frequency analysis. J. Hydrol. 225, 92–101.
Patro, S., Chatterjee, C., Singh, R., Raghuwanshi, N.S., 2009. Hydrodynamic modelling of a large flood-prone river system in India with limited data. Hydrol. Process. 23 (19), 2774–2791.
Pfaundler, M., 2001. Adapting, Analysing and Evaluating a Flexible Index Flood Regionalisation Approach for Hetero-geneous Geographical Environments. Schriftenreihe des Insti-tutes fur Hydromechanik und Wasserwirtschaft ETH Zurich, Zurich.
Rao, A.R., Hamed, K.H., 1997. Regional frequency analysis of Wabash river flood data by L-moments. J. Hydrol. Eng. 2 (4), 169–179.
Rodriguez-Iturbe, I., Rinaldo, A., 1997. Fractal River Basins. Cambridge Univ. Press, Cambridge, UK.
Sanders, B.F., 2007. Evaluation of on-line DEMs for flood inundation modeling. Adv. Water Resour. 30 (8), 1831–1843.
Sarhadi, A., 2008. Incorporating RS & GIS Techniques and Frequency Analysis Models for Flood Inundation Study at JIROFT Vicinity. M.Sc. Dissertation, Isfahan University of Technology, Isfahan, Iran.
Sarhadi, A., Modarres, R., 2011. Flood seasonality-based regionalization methods: a data-based comparison. Hydrol. Process. 25 (23), 3613–3624.
Schumann, G., 2007. High-Resolution 3-D flood information form radar imagery for flood hazard management. IEEE Trans. Geosci. Remote Sens. 45 (6), 1715–1725.
Singh, V.P., 1992. Elementary Hydrology. Prentice-Hall, Englewood Cliffs, NJ, pp. 824–829.
Smith, K., 2001. Environmental Hazards Assessing Risk and Reducing Disaster, third ed. Routledge 11 New Fetter Lane, London.
Srinivas, V.V., Tripathi, S., Rao, A.R., Govindaraju, R.S., 2008. Regional flood frequency analysis by combining self-organizing feature map and fuzzy clustering. J. Hydrol. 348, 148–166.
Straatsma, M.W., Baptist, M.J., 2008. Floodplain roughness parameterization using airborne laser scanning and spectral remote sensing. Remote Sens. Environ. 112 (3), 1062–1080.
U.S. Army Crops of Engineers, H.E.C., 2003. HEC-RAS User Manual. Davis, CA.
Vogel, R.M., McMahon, T.A., Chiew, F.H.H., 1993. Flood flow frequency model selection in Australia. J. Hydrol. 146, 421–449.
Vogel, R.M., Wilson, I., Daly, C., 1999. Regional regression models of annual streamflow for the United States. J. Irrigat. Drain. Eng. 99 (3), 148–257.
Wahren, A., Feger, K.H., Schwärzel, K., Münch, A., 2009. Land-use effects on flood generation – considering soil hydraulic measurements in modelling. Adv. Geosci. 21, 99–107.
Webster, T.L., Forbes, D.L., Dickie, S., Shreenan, R., 2004. Using topographic LiDAR to map flood risk from storm-surge event for Charlottetown, Prince Edwaed Island, Canada. Can. J. Remote Sens. 30 (1), 64–76.
Wilson, M., 2004. Evaluating the Effect of Data and Data Uncertainty on Predictions of Flood Inundation, University of Southampton, Southampton.